Mineralium Deposita (2018) 53:1095–1116
https://doi.org/10.1007/s00126-018-0797-1

ARTICLE

Nature and origin of the nonsulfide zinc deposits in the Sierra Mojada District, Coahuila, Mexico: constraints from regional geology, petrography, and isotope analyses

J. Richard Kyle[1] · Hyein Ahn[1] · H. Albert Gilg[2]

Received: 1 February 2017 / Accepted: 7 February 2018 / Published online: 20 February 2018

Abstract

The Sierra Mojada District comprises multiple types of near-surface mineral concentrations ranging from polymetallic sulfide zones, "nonsulfide Zn" (NSZ) deposits, and a silver-rich Pb carbonate deposit hosted by lower Cretaceous carbonate strata. Hypogene concentrations of Fe-Zn-Pb-Cu-Ag sulfides and sulfosalts are locally preserved and are associated with hydrothermal dolomite and silica. Alteration mineralogy and sulfur isotope data suggest primary Zn-Pb-Ag mineralization from circa 200 °C hydrothermal fluids. The NSZ deposits dominantly consist of smithsonite and hemimorphite associated with local Mn-Fe oxides. The Red Zinc Zone consists of strata-bound zones dominantly of hemimorphite that fills pores in residual and resedimented Fe oxides. The White Zinc Zone shows local dissolution features, including internal sediments interbanded with and cemented by smithsonite. Similar Pb isotopic compositions of smithsonite, hemimorphite, and cerussite to Sierra Mojada galena document that the NSZ deposits originated from polymetallic carbonate-replacement sulfide deposits, with flow of metal-bearing groundwater being controlled by local topography and structural features in this extensional terrane. Oxygen isotope values for Sierra Mojada smithsonite are relatively constant ($\delta^{18}O_{VSMOW}$ = 20.9 to 23.3‰) but are unusually low compared to other supergene smithsonites. Using $\delta^{18}O_{VSMOW}$ (− 8‰) of modern groundwater at nearby Cuatrociénegas, smithsonite formational temperatures are calculated to have been between 26 to 35 °C. Smithsonite precipitation was favored by near-neutral conditions typical of carbonate terranes, whereas hemimorphite precipitated by reaction with wallrock silica and locally, or episodically, more acidic conditions resulting from sulfide oxidation. Transition to, and stabilization of, the modern desert climate over the past 9000 years from the Late Pleistocene wetter, cooler climate of northern Mexico resulted in episodic drawdown of the water table and termination of local supergene metal mobilization.

Keywords Supergene processes · Smithsonite · Hemimorphite · Carbon-oxygen-sulfur isotopes · Lead isotopes · Polymetallic carbonate-replacement deposits · Holocene climate

Introduction

The Sierra Mojada District in northern Mexico includes polymetallic sulfide deposits, "nonsulfide Zn" (NSZ) deposits, and a silver-rich lead carbonate deposit, hosted by lower Cretaceous carbonate strata. The origin of the hypogene sulfide deposits is enigmatic, but they are typically included in compilations of polymetallic carbonate-replacement deposits (e.g., Megaw et al. 1988, 1996). This study focuses on the two NSZ deposits, which have been referred to as the White Zinc Zone or Smithsonite Manto and the Red Zinc Zone or Iron Oxide Manto (AKF Mining Services 2015; Hodder 2001). The White Zinc Zone shows dynamic dissolution features, including internal sediments interbanded with

Editorial handling: F. Melcher

Electronic supplementary material The online version of this article (https://doi.org/10.1007/s00126-018-0797-1) contains supplementary material, which is available to authorized users.

✉ J. Richard Kyle
rkyle@jsg.utexas.edu

[1] Department of Geological Sciences, Jackson School of Geosciences, University of Texas at Austin, Austin, TX 78712, USA

[2] Lehrstuhl für Ingenieurgeologie, TUM, Arcisstr. 21, 80333 Munich, Germany

smithsonite. The Red Zinc Zone consists of strata-bound zones dominantly of hemimorphite that fills pores in iron oxides and iron-rich oxidized dolostones. In addition to smithsonite and hemimorphite, the NSZ mineralization includes minor hydrozincite and Zn clays (sauconite) associated mainly with calcite and Mn-Fe oxides. Thus, the Sierra Mojada District provides the opportunity to examine the genetic relationships between the two most common types of supergene zinc-forming systems, the "white zinc" (smithsonite-bearing) and "red zinc" (hemimorphite-bearing) deposits (e.g., Hitzman et al. 2003). NSZ concentrations commonly are present in near-surface portions of polymetallic carbonate-replacement deposits in northern Mexico (Megaw 2009, 2010), and thus studies of the Sierra Mojada system may have broader implications to other NSZ mineralization, including the relationship to Holocene regional climatic evolution. Further, the local preservation of polymetallic hypogene zones at Sierra Mojada provides materials to constrain the overall metallogenic system, for which alternative interpretations have been presented (Megaw et al. 1988, 1996; Tritlla et al. 2007; González-Sánchez et al. 2009).

The Sierra Mojada District was discovered in 1879 as high grade silver ores associated with lead carbonates that were mined through the 1950s; this Lead Carbonate Manto is essentially depleted, and little of this style of mineralization remains. The discovery of copper-silver ores in 1906 led to new exploration on the north side of the Sierra Mojada fault. The NSZ deposits were discovered in the 1920s, with further developments resulting in more than 50 historic shafts in the district. Following a period of dormancy or small scale mining, interest in the district resumed in 1997, with property consolidation followed by an extensive drilling program by Metalline Mining Company (Hodder 2001) and a metallurgical study of zinc recovery from oxide ores (De Wet and Singleton 2008). The district has a measured and indicated resource of 58.7 million tonnes grading 3.6% zinc and 50 g/t silver (AKF Mining Services 2015).

Much research has been conducted on metal deposits in northern Mexico, but no recent detailed studies of the Sierra Mojada District ores have been conducted. Several compilations include Sierra Mojada, viewing it either as high-temperature carbonate-replacement mineralization (Megaw et al. 1988, 1996), or given the lack of evidence of intrusive activity and high-temperature mineral assemblages at Sierra Mojada, mineralization related to low-temperature sedimentary basin-related processes (Tritlla et al. 2007; González-Sánchez et al. 2009). Hybrid mineralization models for polymetallic carbonate-replacement deposits also exist whereby the magmatism and mineralization sites are controlled by local tectonic features, but mineralization may involve either or both magmatic and sedimentary brines (Megaw et al. 1996; Kyle 2012). Recent deep drilling in the western end of the Sierra Mojada District has encountered structurally controlled zones of intense silica alteration with hypogene Zn-Pb-Cu-Ag sulfide mineralization interpreted to represent the distal part of a carbonate-replacement system (Silver Bull Resources 2017). The age of the Sierra Mojada carbonate-replacement mineralization is not known, but generally, it would be viewed as a mid-Cenozoic event by comparison with other intrusion-associated polymetallic carbonate-replacement systems in northern Mexico (Megaw et al. 1988).

This study constrains the nature and origin of the Sierra Mojada NSZ concentrations through petrographic study of major Zn-bearing minerals, complemented by laser ablation trace element studies, and carbon and oxygen isotope analysis of carbonate minerals. Petrography of primary sulfide concentrations and sulfur and lead isotope analyses are used to constrain the nature of hypogene mineralization. The Pb isotope compositions of supergene Zn and Pb minerals were determined to assess the genetic relationship between the sulfide and NSZ concentrations.

Regional and district geology

The Sierra Mojada District is located in westernmost central Coahuila, Mexico (N 27.275°, W 103.68°), near the border with the state of Chihuahua (Fig. 1). The mining district extends ~5 km east-west and 1.5 km north-south. Elevations in the district range from about 1300 to 1500 m in the area of the mines, with the crest of the Sierra Mojada at more than 2400 m (Fig. 2a). The district is within the Chihuahuan Desert with an arid to semi-arid climate, averaging ~40 cm of annual precipitation.

The geology of northeastern Mexico is a product of a complex series of tectonic and related events, starting with the Ouachita Orogeny during the late Paleozoic, followed by Jurassic rifting and opening of the Gulf of Mexico with passive margin development through the late Cretaceous (Goldhammer 1991). The regional basement comprises Late Paleozoic metaclastic units that accumulated on the North American craton during the Ouachita Orogeny. The basement is unconformably overlain by Middle Jurassic terrestrial red beds and evaporitic strata (Campa and Coney 1983).

Laramide deformation occurred during the Late Cretaceous through the Early Paleogene (Chávez-Cabello et al. 2007). Northeast-directed Laramide compression formed the Mexican thrust belt in which most polymetallic carbonate-replacement deposits occur (Megaw et al. 1988, 1996), but the margins of the Mexican thrust belt were less folded than the interior where the Sierra Mojada District lies.

The Sabinas Basin and contiguous Coahuila Block originated during a rifting event related to the opening of the Gulf of Mexico (Fig. 1). The northern margin of the Coahuila Block is bound by the San Marcos Fault, a regional basement

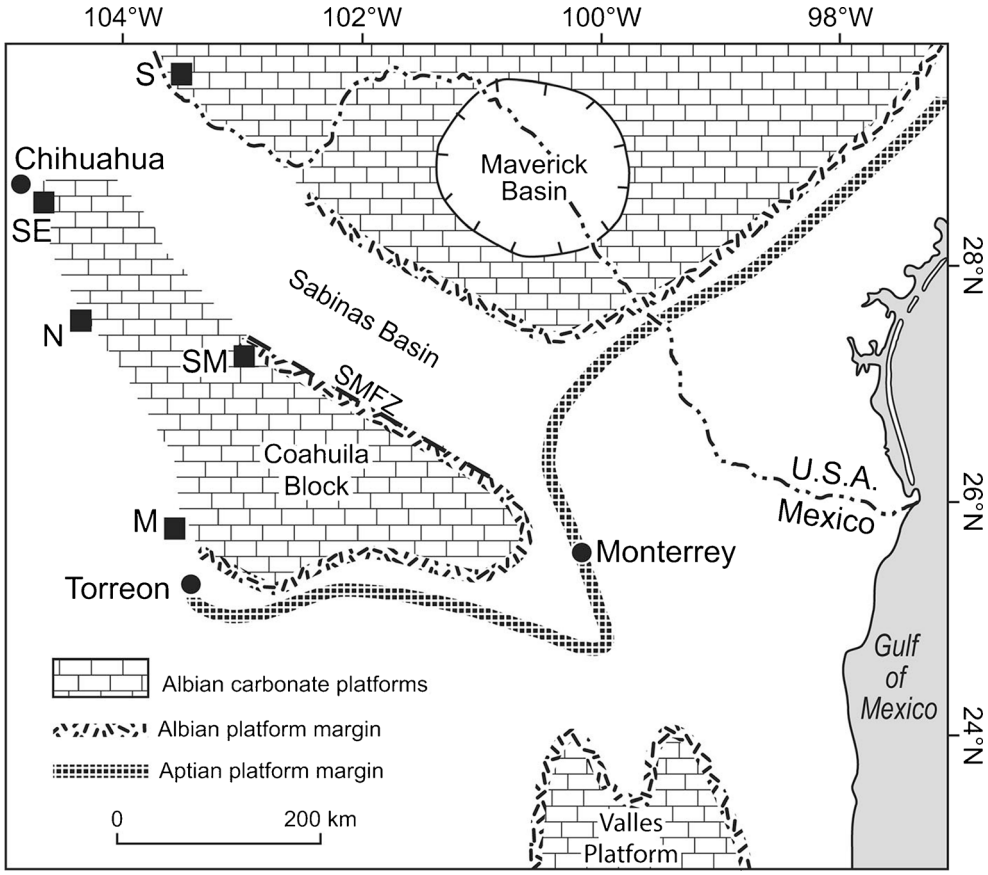

Fig. 1 Location of the Sierra Mojada and selected other polymetallic districts in north central Mexico and the adjacent border region relative to Late Cretaceous carbonate platform margins. M, Mapimi; N, Naica; S, Shafter; SE, Santa Eulalia; SM, Sierra Mojada; SMFZ, San Marcos Fault Zone. Regional Cretaceous geologic framework modified from Lehmann et al. (1999)

structure with a length of at least 300 km that separates the Coahuila Block from the Sabinas Basin (Goldhammer 1991). The fault is believed to have been reactivated at least four times since Late Jurassic extension in response to the opening of the ancestral Gulf of Mexico Basin (Chávez-Cabello et al. 2007).

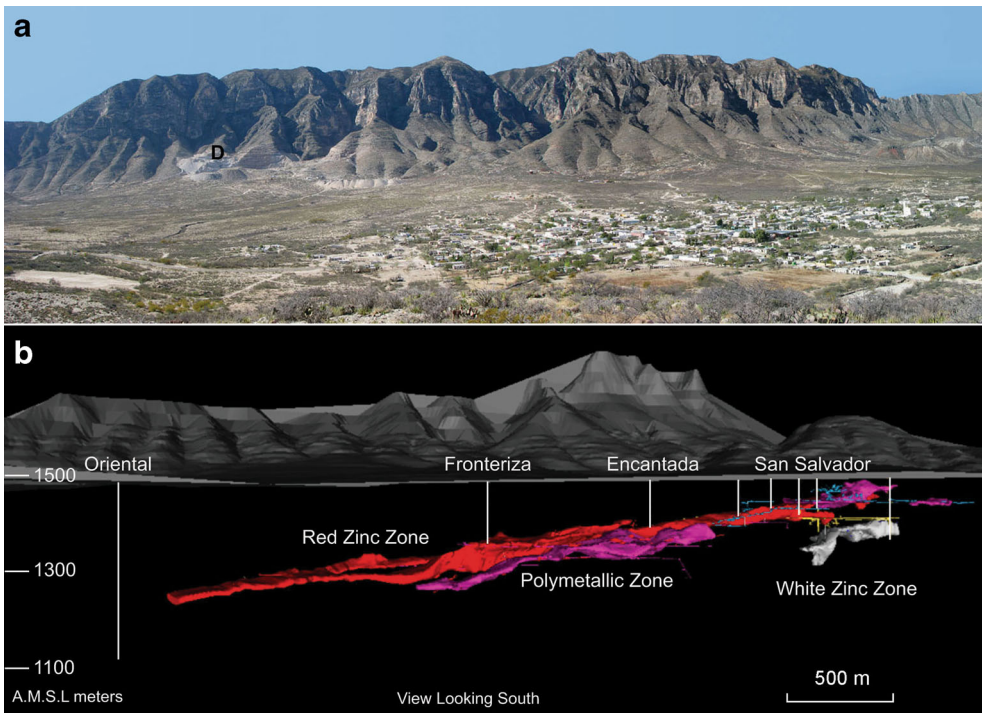

Fig. 2 Orebodies and mines of the Sierra Mojada District. **a** Panorama of the Sierra Mojada range looking south with historic mine workings along the lower slopes. Town of Esmeralda, Coahuila, in the foreground. D = Dolomita quarry. **b** Block model of ore zones in central part of the district looking south, including the Red Zinc Zone, White Zinc Zone, and polymetallic zone. Field of view and orientation is not a direct match to **a**, with generalized surface topography. Modified after Metalline Mining (2008); further exploration has extended and modified the distribution of mineralized zones (AKF Mining Services 2015)

Sierra Mojada is located along the northeastern margin of the Coahuila Block and the northwestern trace of the San Marcos Fault Zone that is locally referred to as the Sierra Mojada fault. The Coahuila Block of Paleozoic to Triassic rocks forms the basement in the Sierra Mojada District. Drilling near the base of the Sierra Mojada has intersected deformed argillite and diorite at a depth of ~ 350 m (Gryger 2010) that is considered to be the Jurassic-Triassic Ouachita basement (Fig. 3). The basement is unconformably overlain by a basal polymictic conglomerate before transitioning into the Mesozoic carbonate succession (Gryger 2010). The ores are hosted by the conglomerate and carbonate strata that historically have been attributed to the upper part of the La Pena Formation and the lower part of the overlying Aurora Group.

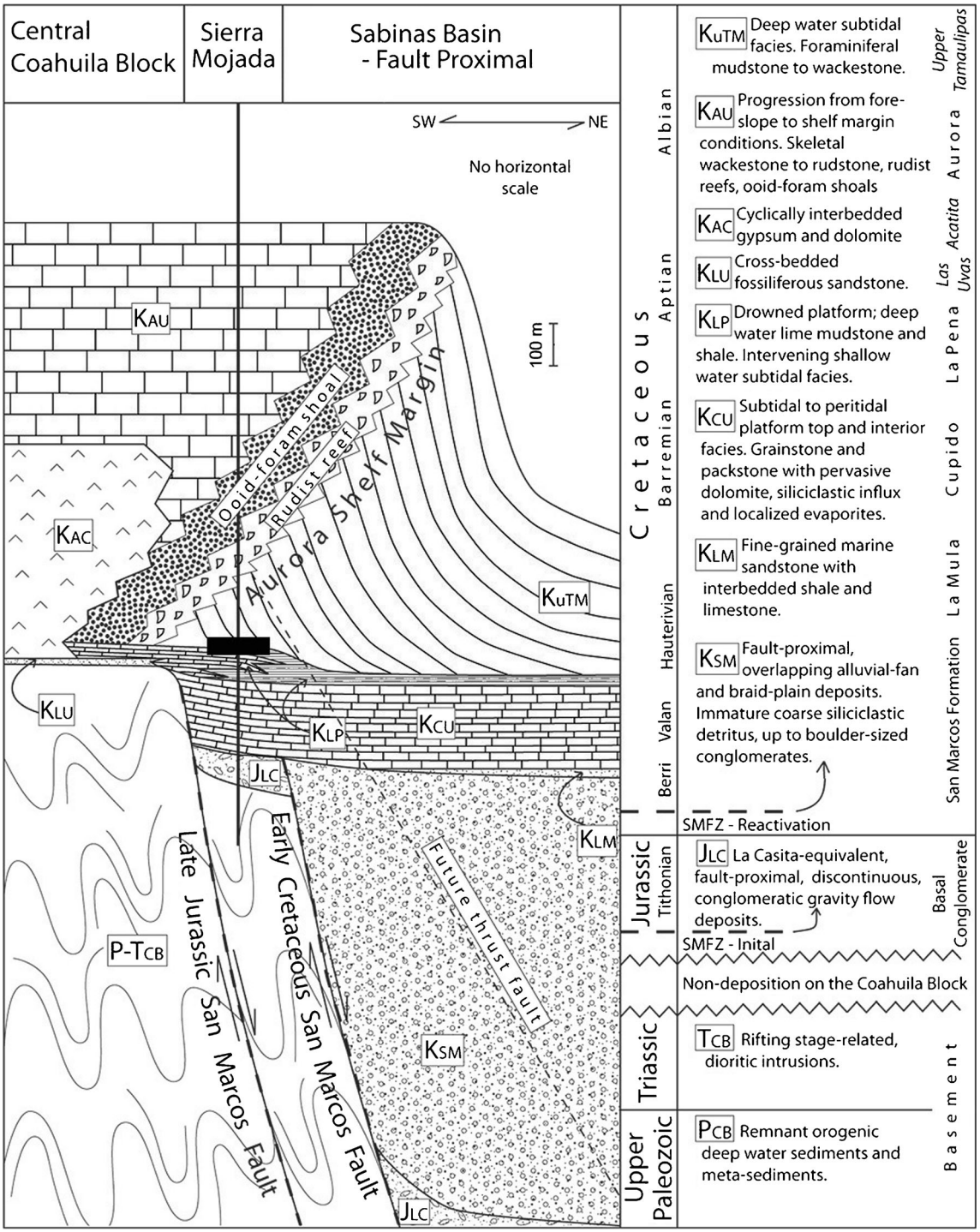

Fig. 3 Schematic section of the geologic relations of the Coahuila Block and Sabinas Basin in the Sierra Mojada region. Solid rectangle represents the general position of Sierra Mojada District mineralization. Modified from Gryger (2010)

The La Pena Formation consists of thin-bedded limestone, whereas the Aurora Group consists of thick massive beds of platform and reef limestone with large rudistid bivalves.

The San Marcos Fault serves as the boundary between the Coahuila Block and the Sabinas Basin (Fig. 1). The paleogeography imposed by these regional elements governed depositional patterns and carbonate platform morphology throughout the Late Jurassic and Early Cretaceous. The Cupido carbonate system filled the Sabinas Basin with shallow water carbonates during the Barremian and Aptian, whereas the Coahuila Block was exposed at this time. A major Aptian transgression marks the end of the Cupido platform and the beginning of the Aurora platform. During the Albian, carbonates were restricted to the topographically elevated Coahuila Block, with Sierra Mojada located on its topographic margin. The Sierra Mojada succession records the evolution of the proximal Cupido platform and its subsequent inundation (Gryger 2010).

The Sierra Mojada NSZ deposits are hosted by the Cretaceous carbonate sequence south of the Sierra Mojada fault. The tabular mineralized zone dips ~ 10° eastward underlying the northern flank of the Sierra Mojada range (Fig. 2). The mineralized zone cropped out at ~ 1500 m and extends to ~ 1200 m elevation in a region where the highest local elevation is 2400 m in the Sierra Mojada to the south. The current water table is below known Zn orebodies in the district, even for the deepest mine workings at 1135 m elevation. Wells in carbonate strata around the mine area are nonproductive, but artesian wells occur in the carbonate sequence several kilometers away from the mine area where the water table is at ~ 1000 m elevation. The water is sulfate-bicarbonate-chloride type with a temperature of 26–27 °C and near neutral (6.7–7.4) pH (R. Kolvoord, 2009, written commun.).

Mineral deposits of the district

The Sierra Mojada District comprises four major mineralization styles: polymetallic (Fe-Zn-Pb-Cu-Ag) sulfides and two nonsulfide Zn deposits, White Zinc Zone or Smithsonite Manto and the Red Zinc Zone or Iron Oxide Manto, as well as the historic silver-rich Lead Carbonate Manto. The NSZ and Lead Carbonate Manto occur in lower Cretaceous carbonate strata south of the Sierra Mojada fault (Fig. 1).

The Lead Carbonate Manto was the original Sierra Mojada discovery and was essentially depleted in 1905 after producing more than 3 Mt of ore averaging ~ 15% Pb and ~ 400 g/t Ag (Shaw 1922). The Lead Carbonate Manto was hosted in the carbonate strata of the middle Aurora Group, stratigraphically above the Red Zinc Zone in the lower Aurora. The Lead Carbonate Manto was mined along a northeast-striking structure for ~ 4 km and was up to 30 m wide and 6 m thick (Shaw 1922). The Lead Carbonate Manto workings are essentially inaccessible, and only a few cerussite-rich ore samples were available for this study.

The Red Zinc Zone (Fig. 2b) extends for at least 2.5 km along strike in the footwall of the Sierra Mojada fault and averages ~ 80 m thick and ~ 130 m wide. The Red Zinc Zone consists of strata-bound bodies of Fe-oxide-rich material with Zn-bearing silicates and carbonates within a dolomitic zone in the lower Aurora Group (Fig. 3). The complex White Zinc Zone underlies the Red Zinc Zone and consists of two fault-separated bodies in the basal Aurora Group 100–200 m wide and up to 70 m thick (Fig. 2b). The thickest section of the Red Zinc Zone directly overlies the White Zinc Zone where the total zinc zone is more than 200 m thick (AKF Mining Services 2015).

Hypogene polymetallic sulfide concentrations

Sulfide minerals are only locally preserved and commonly even those occurrences are partially oxidized. Two types of sulfide-bearing materials are present: polymetallic sulfides that commonly cement breccia (Fig. 4a, b), but can be locally massive, and disseminated to stylolite-hosted silver-bearing zones in the "shallow silver zone." The latter was not investigated in detail in this study and will not be discussed further.

Nonsulfide Zn mineralization

The two main nonsulfide Zn deposits, the White Zinc Zone and the Red Zinc Zone, consist of stratigraphically constrained Zn carbonates and silicates. The most abundant NSZ minerals are smithsonite and hemimorphite, with lesser concentrations of hydrozincite and sauconite. Minor amounts of Mn oxides commonly are intergrown with smithsonite and Zn clays. Late-stage calcite is abundant in both NSZ deposits, along with minor amounts of barite.

The NSZ zones are spatially separated from each other and from the polymetallic sulfide zone (Fig. 2b). The Red Zinc Zone extends more than 2 km from surface exposures in the western part of the district at ~ 1500 m elevation towards the east at ~ 10°. The zone is broadly strata-bound with pore-filling of hemimorphite and smithsonite in iron oxide-rich materials, including local cave-fill deposits. Hemimorphite and smithsonite in the Red Zinc Zone are hosted by dolomitic goethitic or hematitic oxide matrix. In many cases, hemimorphite is coated by late-stage calcite that also occurs in pores that do not contain hemimorphite.

The White Zinc Zone occurs between 1300 and 1400 m elevation underlying the Red Zinc Zone (Fig. 2b). Our studies were dominantly of relationships observed and samples collected from the accessible lowermost zone. The White Zinc Zone has a chimney-like morphology with a maximum dimension of ~ 400 m and shows dynamic dissolution features with internal sediments cemented by smithsonite,

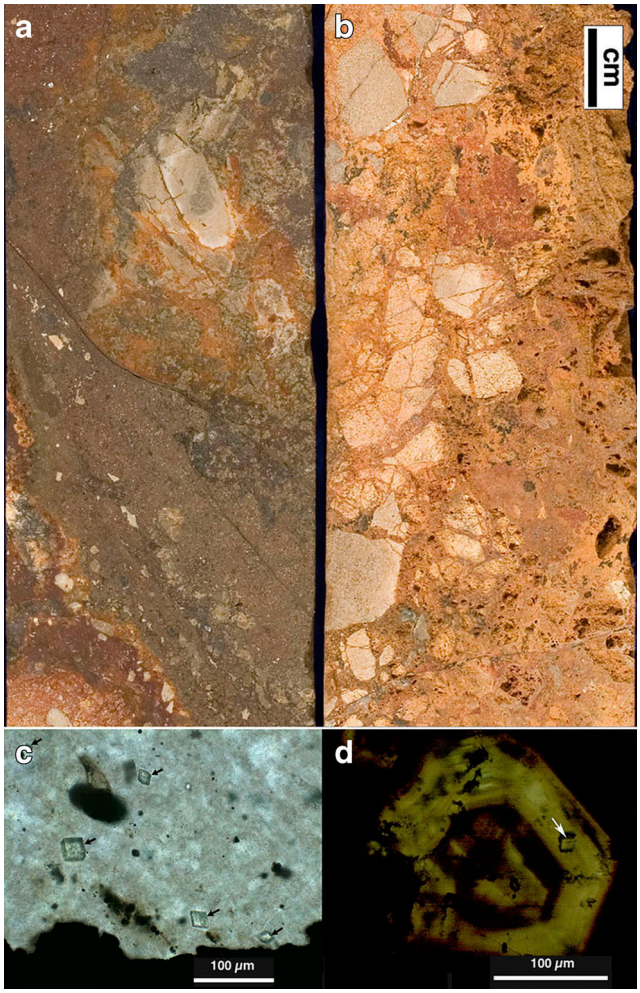

Fig. 4 Polymetallic mineralization and hypogene alteration features. **a** Partly oxidized dolostone breccia cemented by iron sulfides, sphalerite, and galena. **b** Leached polymetallic breccia zone from same core. **c** Microcrystalline silica encasing dolomite rhombs (arrows). **d** Zoned sphalerite encasing dolomite rhomb (arrow)

hemimorphite, or calcite (Fig. 5). Smithsonite forms local colloform to banded masses as much as 25 cm thick (Megaw 2009, 2010) where open space was available. Cave-fill sediments contain sauconite and Mn-Fe oxides locally cemented by hemimorphite or calcite. These sedimentary materials are composed of friable fine-grained sediments and clay fragments (Fig. 5c, d). Botryoidal smithsonite with minor amounts of hemimorphite commonly occurs in vuggy macropores (Figs. 5d–f and 6). Smithsonite bands are commonly subhorizontal, but vertical smithsonite bands are locally present in the White Zinc Zone.

Sampling and methodology

During five visits to the Sierra Mojada District from 2003 to 2009, several hundred samples were collected from underground and surface sites and from cores in the Red Zinc and White Zinc ore zones, as well as from cores that intersected locally preserved sulfide mineral zones. Petrographic sections of Zn carbonates, Zn silicates, and associated minerals were studied using transmitted and reflected light petrography, cathodoluminescence (CL) petrography, and scanning electron microscopy (SEM) with an energy-dispersive X-ray detector (EDS) at the University of Texas at Austin. Secondary and backscatter electron (BSE) images and elemental spectra were collected with an accelerating voltage between 15 and 30 keV using a JEOL JSM-6490 LV SEM with EDS. For cathodoluminescence petrography of smithsonite, polished thin sections were studied on a Technosyn cold-cathode instrument with operating conditions between 16–22keV and 400~600 μA of accelerating voltage and gun current, respectively; CL response was recorded with Olympus digital camera.

Carbon and oxygen isotopes of smithsonite and calcite were analyzed at the stable isotope laboratory of the Museum für Naturkunde, Berlin, Germany. The CO_2 was extracted from 100 to 400 μg of carbonate by reaction with anhydrous phosphoric acid at 72 °C for about 1.5 h using a Thermo Finnigan GASBENCH II coupled online with a Thermo Finnigan DELTA V isotope ratio mass spectrometer in a continuous He flow mode. Isotope values are reported in the conventional δ-notation in per mil (‰) relative to the standards VSMOW for oxygen and VPDB for carbon. Reproducibility of replicate measurements of lab standards (limestone) is generally ≤ 0.1‰ (one standard deviation). The phosphoric acid fractionation factors used for smithsonite and cerussite were those of Gilg et al. (2003). Sulfur isotopes were determined for mm-scale mineral grain separates at the Stable Isotope Research Facility at Indiana University and are reported in δ-notation in per mil (‰) relative to the VCDT standard; internal standards and replicates indicate precision of ~ 0.1‰.

The TIMS facility at the University of Texas at Austin was used for the common lead isotope analysis of Pb and Zn minerals. Visually pure mineral separates of each sample were dissolved in concentrated HCl to produce an aliquot estimated to contain ~ 100 ng of Pb that was transferred to a separate Teflon vial and dried. Pb was isolated using 200 μL of Bio Rad AG 1-X8, 100–200 mesh, anion resin in a Teflon shrink-tube column. The galena samples were put through the columns once using 0.5 M HBr–0.5 M HNO_3. The cerussite sample was put through the column twice using 1 M HBr–2 M HCl–6 M HCl. Because of their low Pb contents, smithsonite and hemimorphite samples were put through the column twice using 0.5 M HBr–0.5 M HNO_3, then two more times using 1 M HBr–2 M HCl–6 M HCl. Samples were loaded onto outgassed Re filaments with silica gel and 0.3 M H_3PO_4. Pb isotope ratios were measured with a Thermo Triton TI thermal-ionization mass spectrometer in static-multicollection data-acquisition mode. Following Luhr et al. (1995), analytical uncertainty is estimated to be ± 0.05%

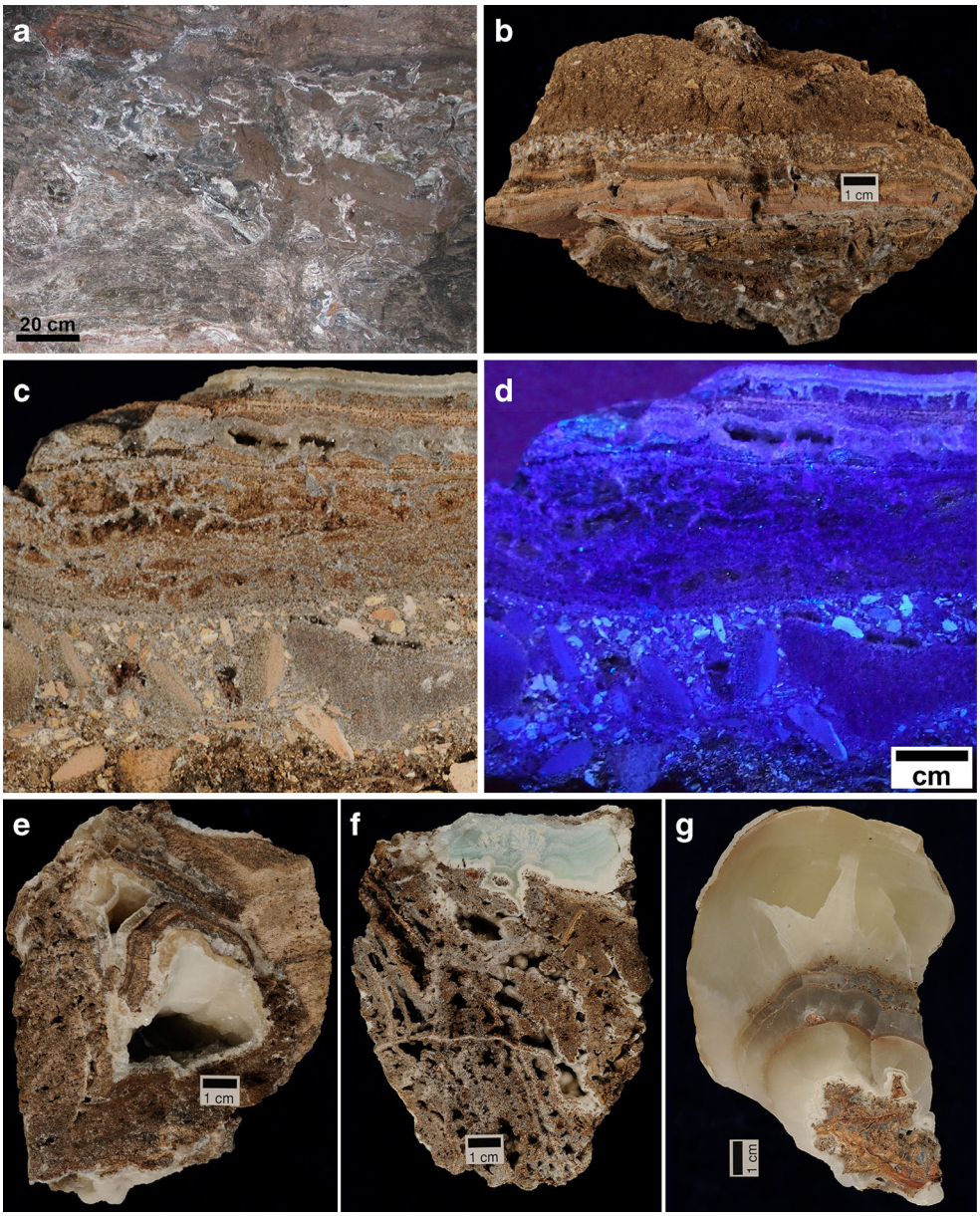

Fig. 5 Features of the White Zinc Zone NSZ mineralization. **a** Underground exposures of the lower levels of the White Zinc Zone showing irregular smithsonite bands interbanded with pebble to clay size dolomitic residue zones. **b** Fragments and layers of Zn clay (pink to pale brown colors) cemented by Zn-bearing minerals and calcite. **c** Irregular bands and stringers of smithsonite in cave fill detritus including polymictic breccia zone. **d** Shortwave UV photo of **c** showing weakly fluorescing smithsonite and variable carbonate and Zn clay clast fluorescence. **e** Pores in cave fill lined by botryoidal smithsonite. **f** Irregular vuggy cave-fill with pores lined by white fine-grained hydrozincite and greenish blue smithsonite. **g** 10-cm thick botryoidal smithsonite on detrital substrate

per amu (2σ), which is equivalent to ± 0.0004 for typical $^{207}Pb/^{206}Pb$ ratios, ± 0.002 for $^{208}Pb/^{206}Pb$ ratios, ± 0.02 for $^{206}Pb/^{204}Pb$ ratios, ± 0.02 for $^{207}Pb/^{204}Pb$ ratios, and ± 0.08 for $^{208}Pb/^{204}Pb$ ratios. The average reproducibility of 14 duplicate analyses of four different samples is 0.026% per amu.

Results

Petrography

Polymetallic sulfide deposits

Based on the study of limited polymetallic zone samples, the principal sulfide minerals are sphalerite, galena, pyrite, and marcasite, with local tetrahedrite-tennantite group minerals. Covellite is present locally, replacing other metallic minerals, notably the sulfosalts, and is interpreted to represent secondary mobilization of Cu.

Dolostones are the dominant strata within the Sierra Mojada District, possibly related to refluxing of Cretaceous evaporative brines off the Coahuila Block as suggested by the Acatita Formation (Fig. 3; Lehmann et al. 1999). These regional dolostones do not appear to be related to the hypogene mineralizing event, except to provide increased intrastratal porosity and permeability to facilitate fluid flow.

Local transgressive and pore-filling zones of ferroan dolomite within the host units appear to be hydrothermal, but the relationship to polymetallic mineralization is not well constrained. However, dolomite rhombs occur within the

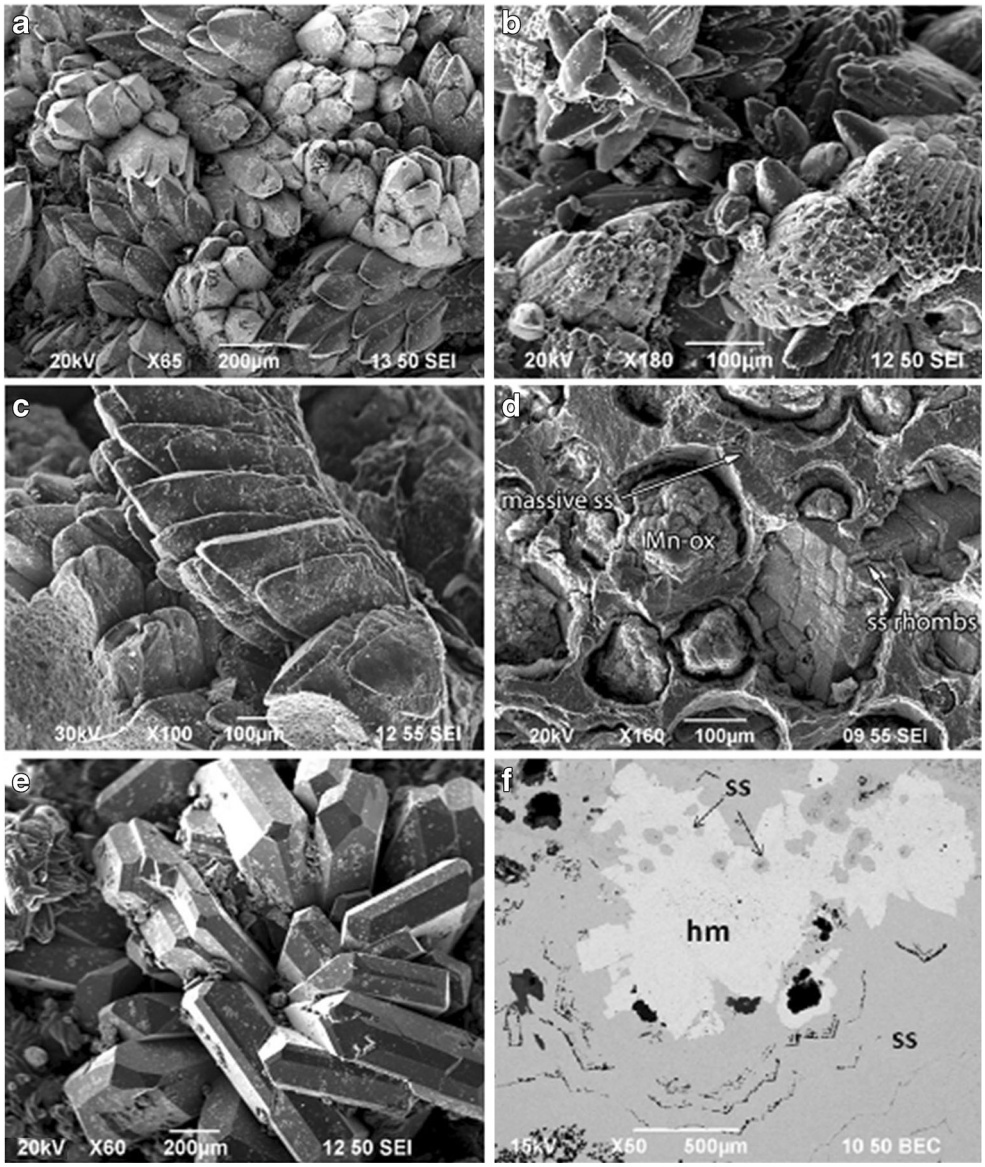

Fig. 6 SEM photomicrographs of smithsonite and other minerals in the White Zinc Zone. **a** Scalenohedral smithsonite. **b** Aggregates of scalenohedral smithsonite and single scalenohedral smithsonite crystal with curved faces. **c** Rhombohedral smithsonite. **d** Rhombic smithsonite and Mn oxides in massive smithsonite. **e** Tabular hemimorphite. **f** Irregular early hemimorphite overgrown (and replaced?) by colloform smithsonite

microcrystalline quartz (Fig. 4c) and within zoned sphalerite (Fig. 4d); thus, dolomite must have been precipitating at the time of sulfide mineralization and related alteration.

Silica is variably abundant in the district, most in the form of chert resulting from diagenetic processes. However, local occurrences of microcrystalline quartz appear to be associated with hydrothermal dolomitization and metallic mineralization (Fig. 4). The presence of widespread silica in the host sequence and primary ore provides a ready silica source for secondary Zn silicates.

White Zinc Zone

Smithsonite in the Sierra Mojada White Zinc Zone is characterized by four morphologies: scalenohedral, rhombohedral, matrix, and massive banded to colloform. The most common type of smithsonite in pores and vugs is an aggregate of scalenohedra growing on a microcrystalline smithsonite and sauconite substrate (Fig. 6). It occurs as either a cluster on smithsonite and sauconite matrix or scalenohedral crusts on smithsonite bands (5 to 10 mm), with the length of scalenohedra ranging from 50 to 400 μm. Aggregates of scalenohedral smithsonite consist of multiple microcrystals (Fig. 6a, c); most scalenohedral smithsonite shows a euhedral crystal surface, although some appear to be etched. The matrix of Zn clays and Mn oxides locally is cemented by smithsonite.

Aggregates of rhombohedral smithsonite crystals (Fig. 6d) form botryoidal smithsonite, typically growing on a massive smithsonite substrate. Colloform smithsonite with a thickness ranging from 5 mm to more than 10 cm is common in vugs (Fig. 5g). On the mineral surface, they are encrusted by Zn clays, Mn oxides, and Fe oxides (Fig. 6d). Colloform

smithsonite typically is white to pale gray, but pale green, blue, and purple varieties are present locally. Zonation is not distinctive in most petrographic sections, but cathodoluminescence reveals striking growth bands at a variety of scales.

Sierra Mojada smithsonite displays a wide range of CL colors from bright pink, red, dull red, violet, and blue (Fig. 7). Smithsonite-A shows consistent blue colors without distinct zonation suggesting that it formed under relatively uniform conditions. Colloform late-stage smithsonite-B, however, demonstrates complex zonation with varying CL colors that LA-ICP-MS analyses confirm is due principally to varying Mn contents (Ahn 2010), as documented for other smithsonite occurrences by Götte and Richter (2004).

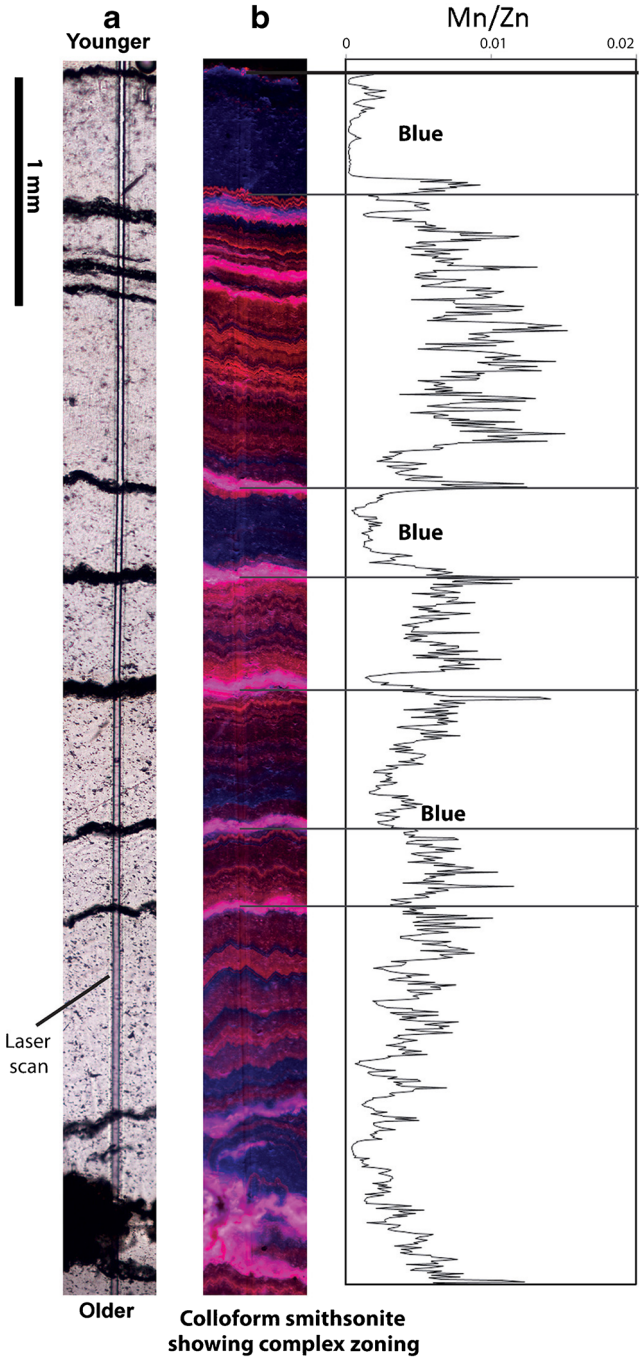

Fig. 7 Banded smithsonite showing CL response and Mn/Zn variation. **a** Polarized light photomicrograph showing laser ablation line scan. **b** Cathodoluminescence photomicrograph of the same traverse showing red and pink bands corresponding to higher Mn contents

Hemimorphite is the second most common NSZ mineral in the White Zinc Zone and is closely associated with smithsonite, calcite, and sauconite. It typically occurs as distinct euhedral (tabular) crystals (Fig. 6e). Hemimorphite occurs as two distinct morphological types that are termed hemimorphite-A and hemimorphite-B. Hemimorphite-A occurs as subhedral to euhedral crystals replacing or intergrown with smithsonite and filling fractures in NSZ ore zones. It shows fan-shaped mineral habits in petrographic section (Fig. 6f) and appears to have partially replaced banded smithsonite along certain layers or along fractures in smithsonite.

Hemimorphite-B occurs as pore-filling tabular hemimorphite (Fig. 6e) that may be locally altered to sauconite or overgrown by calcite. It is also found on the outer edge of smithsonite as single or multiple crystals. Cell parameters for selected hemimorphite from XRD analyses are 8.370, 10.719, and 5.120 Å (Ahn 2010), similar to values reported by Boni et al. (2003).

Hydrozincite appears to be relatively uncommon compared to other secondary Zn minerals. It is locally present in association with smithsonite as white pulverent bands up to several millimeters thick or late coatings, as well as locally dendritic growths within smithsonite (Fig. 5f).

Although not a focus of this study, Zn-bearing clay minerals (Mondillo et al. 2015; Choulet et al. 2016) have been observed with smithsonite and hemimorphite in most White Zinc Zone samples (Fig. 8). The dominant clay mineral tentatively is identified as sauconite, the Zn-dominated smectite (Ross 1946). Sauconite typically has a powdery texture and is variably pink, white, ivory, or bright brown. Sauconite displays various mineral habits, including globular, fibrous, rosette, and massive forms. Even combining megascopic observation, thin section petrography, and SEM-EDS spectra, identification of specific clay minerals proved to be a challenge. In particular, the elemental peak overlap between Na and Zn made it difficult to resolve the relative abundance of Na vs. Zn (Buatier et al. 2016).

Thin section petrography and SEM-EDS analyses reveal that hemimorphite and smithsonite have been replaced locally by sauconite (Fig. 8). Scalenohedral smithsonite is locally replaced by Zn clays and Mn minerals (Fig. 8b) which may have grown on Zn clay matrix. Some of these Mn-bearing Zn clays show variable morphological types and EDS patterns. Sauconite alternating with white-banded smithsonite is present locally (Fig. 5b). Some Zn clay layers appear to be intergrown with smithsonite, but locally Zn clays appear to be clasts within the internal detritus fill (Fig. 5c, d) that are cemented by smithsonite.

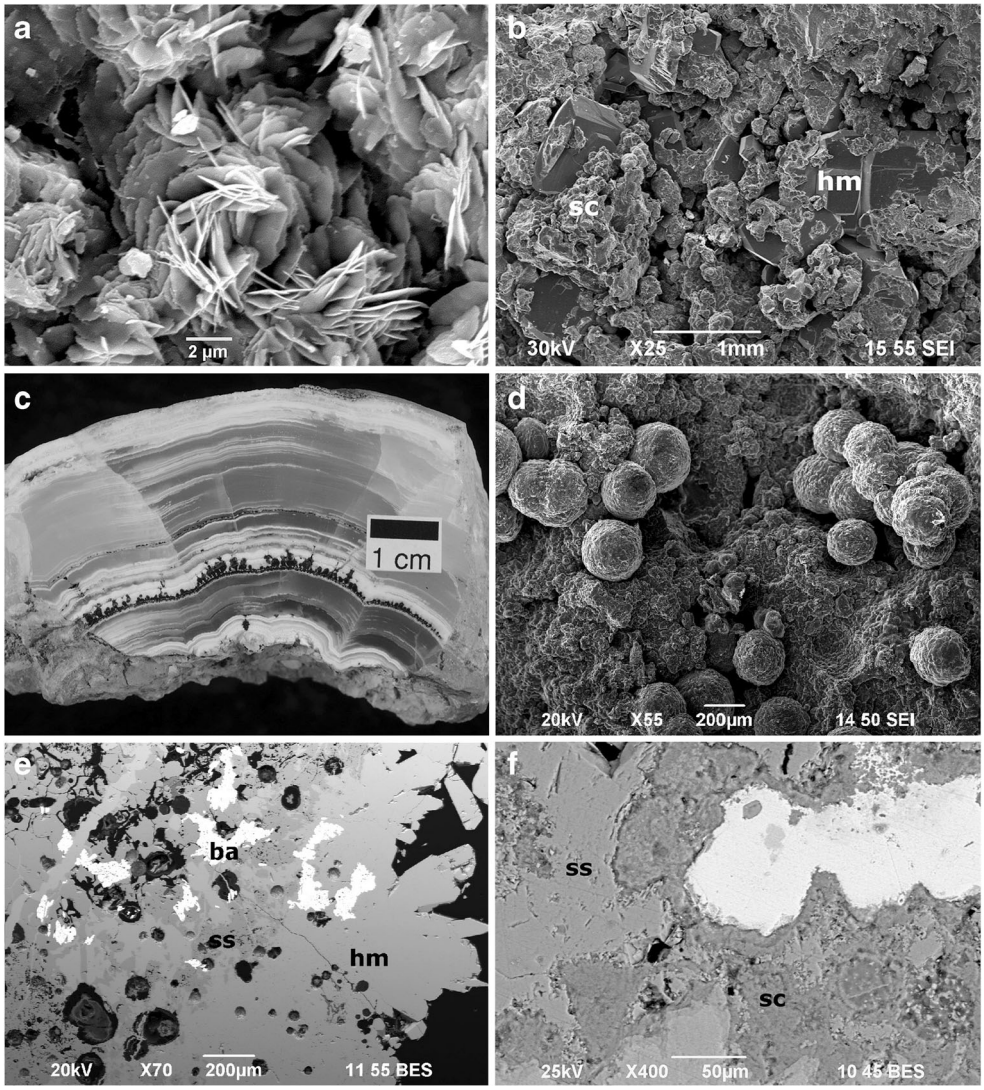

Fig. 8 Petrography of Zn clays and other NSZ-associated minerals. **a** Mn-rich Zn clay showing rosette patterns. **b** Tabular hemimorphite mostly altered to sauconite. **c** Colloform smithsonite with abundant arborescent Fe-Mn oxides. **d** Globular Mn oxides. **e** Smithsonite-barite aggregate overgrown and replaced by hemimorphite. **f** Mn-Pb-bearing mineral (arrow) surrounded by sauconite and smithsonite

Secondary electron images of different types of authigenic Zn clays reveal a variety of elemental peaks, suggesting variable compositions. White clays show Zn, Si, and Al elemental peaks without a Mn peak (Fig. 8a). Pink to brown Zn clays commonly show a Mn peak and are commonly associated with Mn ± Fe oxides (Fig. 8d). K(-Mg)-bearing Zn clays were tentatively identified as fine-grained intergrowths with other mineral phases. Barite is relatively common in the White Zinc Zone (Fig. 8e), in addition to Mn-Pb-bearing minerals (Fig. 8f).

Red Zinc Zone

The Red Zinc Zone is strata-bound within the basal dolostone unit of the Aurora Group and consists dominantly of pore-filling hemimorphite and smithsonite in Fe oxide matrix (Figs. 9 and 10). In general, Fe oxides with red color are due to hematitic (α-Fe_2O_3) contents and with orange color due to goethitic (α-FeOOH) contents (Fig. 9). In the Red Zinc Zone, hemimorphite is more abundant than smithsonite, and Zn mineralization is followed by late-stage calcite.

Abundance of Fe oxides is a distinctive feature of the Red Zinc Zone. Secondary electron imaging reveals that most Fe oxides are massive, extremely fine-grained, or featureless (Fig. 10). BSE images of Fe oxides show that some primary dolomite textures appear to be preserved (Fig. 10a). Fe oxides also display concentric, colloform textures (Fig. 10b, c) that may represent former sulfide-rich zones.

Hemimorphite in the Red Zinc Zone shows tabular crystal habits in vugs and open spaces (Fig. 9). The size of pore-filling hemimorphite ranges from 200 μm to 1 cm (Fig. 9e). Some hemimorphite has distinct crystal faces, whereas others showing rounded crystal edges overgrown by Fe oxides or late calcite. Subhedral to anhedral hemimorphite is closely associated with, and appears to be locally corroded or replaced by, Fe oxides. Late-stage calcite partially or completely fills pores or coats hemimorphite. BSE imaging combined with EDS analyses of hemimorphite crystals reveals that it contains variable

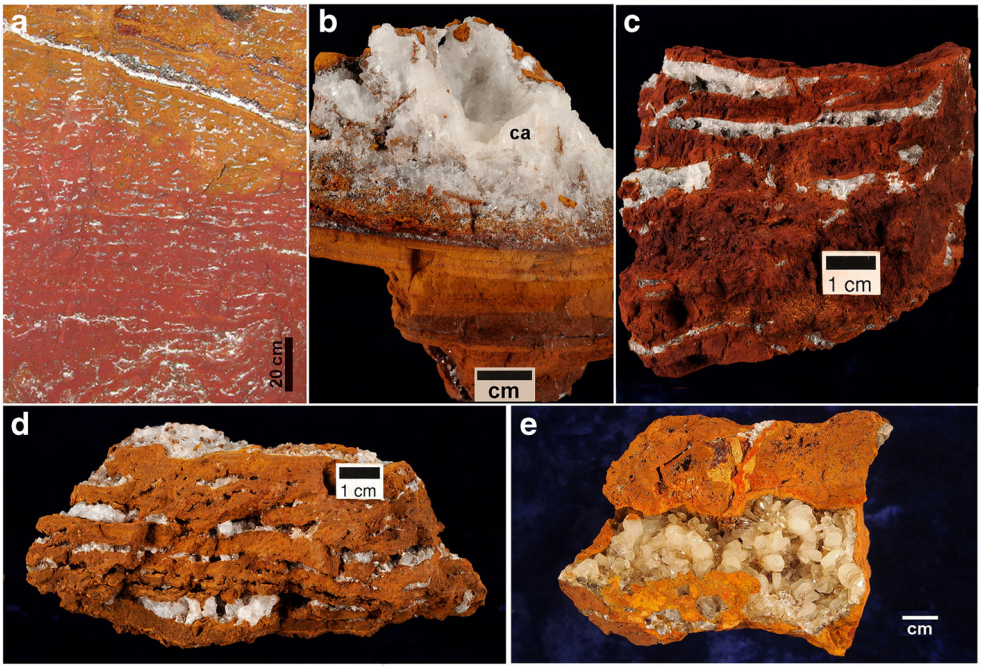

Fig. 9 Features of the Red Zinc Zone NSZ mineralization. **a** Underground exposure of the Red Zinc Zone showing white hemimorphite and calcite crystals in tabular vugs within iron oxide-rich matrix. Yellow goethitic zone is superimposed over the RZZ and appears to be related to a prominent calcite-filled fracture. **b** Hemimorphite and calcite in vugs in laminated Fe oxides. **c** Hematitic Fe oxides with white hemimorphite and calcite crystals. **d** Hemimorphite and calcite crystals in subhorizontal pores in goethitic Fe oxides. **e** Radiating and tabular hemimorphite crystals in a vug

amounts of Ca. In BSE images, the surface of hemimorphite is porous and shows slight compositional variations. These features are absent in the hemimorphite from the White Zinc Zone, suggesting genetic or temporal differences. Small grains of acanthite are present in hemimorphite crystals within goethite.

Smithsonite is much less abundant than hemimorphite in the Red Zinc Zone samples studied. Smithsonite was observed in dark red Fe oxides and in pale orange limestone, but not in the orange Fe oxides. Smithsonite in dark red Fe oxides occurs as rhombic and platy microcrystals with a size ranging from 10 to 100 μm. Globular smithsonite aggregates consisting of platy smithsonite microcrystals have grown on Fe oxide substrate and are overgrown by large tabular crystals of hemimorphite (Fig. 10d), and microcrystals of rhombohedral smithsonite have grown in pores on Fe oxides (Fig. 10e). The size of individual smithsonite crystals ranges from 50 to 100 μm and each cluster is about 200 μm. Smithsonite in fractures in partially oxidized limestone shows distinct compositional variations in BSE images.

Late pore-filling calcite associated with hemimorphite is common in most samples collected from the Red Zinc Zone (Fig. 9). It completely or partially cements pore space around hemimorphite. Barite is common in minor amounts in the Red Zinc Zone samples as euhedral crystals ranging from 50 to 100 μm. Rare colloform Pb-Mn-bearing minerals with Zn are present within the RZZ (Fig. 8f).

Paragenesis

Although the mineral assemblages present in both NSZ zones are relatively similar, a definitive paragenetic relationship between the same minerals in the two zones could not be established. Thus, separate paragenetic sequences are presented for the White Zinc Zone and the Red Zinc Zone (Fig. 11).

Smithsonite was the earliest mineral precipitated in the White Zinc Zone, forming scalenohedra in pores. Hemimorphite-A, sauconite, and Mn oxides are locally associated with early smithsonite in the matrix, suggesting these represent an early mineralization stage. Sauconite is abundant as fragments or laminated with smithsonite and hemimorphite in cave-fills, and occurs as globular forms with smithsonite and hemimorphite. Sauconite occurs on smithsonite-A and hemimorphite-B, suggesting they were locally altered to sauconite.

Tabular hemimorphite-B precipitated in pores and filled some fractures crosscutting smithsonite-A, smithsonite-B, and sauconite during a later stage. Hemimorphite-B also replaced smithsonite locally. Pore-filling hemimorphite crosscuts subhedral barite grains indicating barite precipitated before late hemimorphite. Calcite occurs on hemimorphite and smithsonite indicating it formed after the major nonsulfide Zn mineralization.

In the Red Zinc Zone, smithsonite and hemimorphite are hosted by Fe oxide concentrations. Smithsonite is finely intergrown with Fe oxides indicating it precipitated during the early stage of mineralization. Tabular hemimorphite precipitated on Fe oxides or smithsonite, and locally filled fractures crosscutting smithsonite, Fe oxides, and barite. Pb minerals (Pb oxides and Pb carbonates) locally occur on hemimorphite. Anhedral crystals of barite are found with Fe oxides or as filling fracture in smithsonite; euhedral barite also occurs in fractures in oxidized limestone. These features

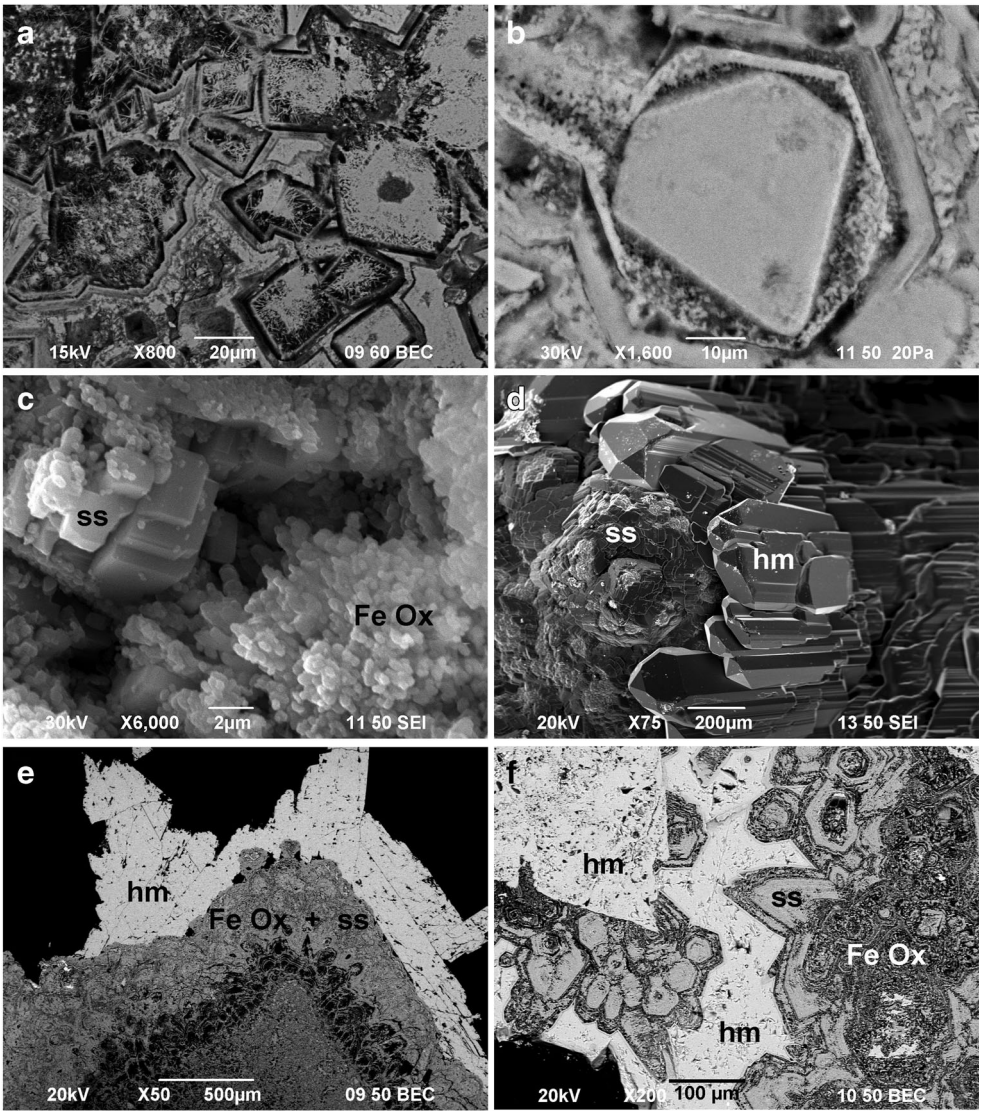

Fig. 10 SEM photomicrographs of hemimorphite and other minerals in the Red Zinc Zone. **a** Dark red iron oxide matrix showing corroded crystals. **b** Fe oxides pseudomorphing a pyrite crystal? **c** Fe oxides and rhombohedral smithsonite. **d** Aggregates of platy smithsonite on Fe oxide substrate and overgrown by hemimorphite. **e** Smithsonite finely intergrown with Fe oxides overgrown by hemimorphite. **f** Smithsonite on Fe oxides cemented by hemimorphite

a White Zinc Zone

Mineral	Early	Late	Occurrences
Smithsonite-A	———		microcrystalline, scalenohedral, rhombohedral, and bands with scalenohedral crusts - dominantly blue CL color
Smithsonite-B	———		banded, massive or colloform - various CL colors
Hemimorphite-A	—		sheaf-like (fibrous) texture - non-luminescent
Hemimorphite-B	- - - - -	———	tabular pore-filling - non-luminescent
Sauconite	——	———	globular, chalky, brown, white or pink - non-luminescent
Calcite		——	white to colorless, fracture- or pore-filling - non-luminescent
Barite		—— -	anhedral - non-luminescent
Mn/Pb minerals	—— - - -		colloform
Mn oxides	—— - - -		globular, colloform locally associated with sauconite

b Red Zinc Zone

Mineral	Early	Late	Occurrences
Hemimorphite	———		tabular pore-filling; fracture-fills
Smithsonite	—— ——		intergrown with Fe oxides -red CL color (early); non-luminescent (late)
Calcite		———	late calcite cement
Barite	—		secondary, euhedral; fracture-fills
Fe-oxides	———		fine-grained, locally crystalline
Mn/Pb minerals	—		colloform or massive

Fig. 11 Paragenetic sequence of NSZ minerals and other common minerals for the **a** White Zinc Zone and for the **b** Red Zinc Zone

suggest that barite was a minor component that likely formed during both primary and secondary mineralization. Calcite cement precipitated after NSZ mineralization and commonly fills pores remaining after hemimorphite precipitation.

Sulfur isotopes

Sulfur isotope analyses of the locally preserved hypogene sulfides and sulfates provide some constraints on the primary mineralization system that is interpreted to be the precursor to the secondary NSZ deposits of the Sierra Mojada District (Table 1). The majority of the sulfide analyses are for galena, because of its better preservation within the partly oxidized ores. The data for sulfides show a bimodal distribution of $\delta^{34}S_{VCDT}$ values with negative (circa −12 ‰) and positive (circa +6 to +8) values. The Acatita anhydrite from a 500-m deep core reveals expected Albian-Aptian seawater $\delta^{34}S_{VCDT}$ values of ~16‰.

Associated sphalerite-galena reveals a $\Delta^{34}S$ value of 3.1‰, suggesting an equilibrium temperature of ~200 °C, similar to a calculated temperature for a barite-galena pair (Table 1), using fractionations of Ohmoto and Goldhaber (1997). Associated pyrite-galena has a somewhat higher calculated temperature, but the paragenetic constraints are not clear. Thus, sulfur isotope fractionation and hydrothermal alteration suggest the Sierra Mojada hypogene mineralization resulted from circa 200 °C fluids.

Carbon and oxygen isotopes of carbonate minerals

Carbon and oxygen isotope data were measured for smithsonite and calcite samples from the White Zinc Zone and calcite from the Red Zinc Zone. These samples include unmineralized limestone, late-stage pore-filling calcite cement from both NSZ deposits, and a calcite speleothem from the White Zinc Zone. Banded, colloform, and scalenohedral varieties of smithsonite from the White Zinc Zone, as well as a sample of massive cerussite from the Lead Carbonate Manto, were analyzed (Table 2).

Calcite

Two limestone samples have $\delta^{13}C$ values of 3.2 and 3.8‰ and $\delta^{18}O$ values of 24.0 and 24.1‰. Average values of late-stage calcite in the White Zinc Zone are $\delta^{18}O$ of 21.7 ± 0.4‰ and $\delta^{13}C$ of −6.3 ± 0.7‰ ($n = 8$), distinct from host limestones (Fig. 12). Different textural or paragenetic types of calcite were analyzed in several samples (Table 2). Commonly, these samples reveal only limited ranges of $\delta^{18}O$ and $\delta^{13}C$ values with no consistent trends among textural types or paragenesis, suggesting relatively similar conditions for later stage calcite pore-filling.

Calcite samples from the Red Zinc Zone yield average carbon and oxygen isotope values are −6.6 ± 1.9 and 21.0 ± 0.8‰ ($n = 4$), respectively (Table 2). The results reveal a wider range of C-O isotope values compared to calcite from the White Zinc Zone (Fig. 12a).

Smithsonite

The $\delta^{18}O$ values of smithsonite A and B show an average of 21.9 ± 0.5‰, and the $\delta^{13}C$ values vary from −8.4 to 1.1‰ with an average of −1.6‰ ($n = 31$) (Fig. 13; Table 2). Smithsonite-A, including scalenohedra without distinct optical zoning, shows a limited carbon isotope range (−0.3 to 1.1‰; $n = 4$). Smithsonite-B, characterized by colloform mineral habits, shows a much wider range of carbon isotope compositions (−8.4 to 1.0 ‰), overlapping with those of smithsonite-A. A pale purplish smithsonite sample yields the lowest $\delta^{13}C$ value. The oxygen isotope compositions of both smithsonite types show a slight increase from A (21.5 ± 0.3‰) to B (22.0 ± 0.5‰). Five samples containing banded smithsonite-B

Table 1 Sulfur isotope composition of Sierra Mojada District sulfide and sulfate minerals

Sample	Ore zone	Description	Mineral	$\delta^{34}S_{VCDT}$ ‰	$\Delta^{34}S$ ‰	Pair	T (°C)
D7080226-23.9	Polymetallic Manto	Polymetallic sulfides in dolostone breccia	Pyrite	6.8			
D7080226-25.5A	Polymetallic Manto	Polymetallic sulfides in dolostone breccia	Sphalerite	8.8	3.1	sl-ga	~190
D7080226-25.5B	Polymetallic Manto	Polymetallic sulfides in dolostone breccia	Galena	5.6	−0.2	py-sl	
D7080226-25.5C	Polymetallic Manto	Polymetallic sulfides in dolostone breccia	Pyrite	8.6	2.9	py-ga	~290
D9090317-13	Polymetallic Manto?	Galena remnants in oxidized fracture in dolostone	Galena	1.7			
DRMT08-1	Dormitos prospect	cm cubic galena crystal in dolostone	Galena	−11.6			
SM03-4	Veta Rica	Massive coarse-crystalline barite with galena	Galena	−13.0			
SM08-Pb01	Veta Rica	Massive fine-grained galena	Galena	11.5			
SM03-5	Veta Rica	Massive coarse-crystalline barite with galena	Barite	15.8	28.8	ba-ga	~180
E500-505	Coahuila Block	Albian-Aptian Acatita Fm evaporitic anhydrite	Anhydrite	16.8			
E500-506	Coahuila Block	Albian-Aptian Acatita Fm evaporitic anhydrite	Anhydrite	16.7			

Equilibrium fractionation values calculated after Ohmoto and Goldhaber (1997)

Table 2 Carbon and oxygen isotope values of Sierra Mojada carbonate minerals

Sample	Ore zone	Description	Mineral	$\delta^{18}O_{VSMOW}$	$\delta^{13}C_{VPDB}$
D9090307-23.5	Wallrock	Host limestone (Aurora?)	Calcite	24.0	3.2
D9090307-58	Wallrock	Host limestone (Aurora?)	Calcite	24.0	3.8
SM03-1	Dolomita	Blocky ca crystals in Aurora dolomite pore	Calcite	22.1	− 7.5
SM03-24-B	WZZ	ca crystal on ss	Calcite	21.1	− 5.4
SM08-11-A	WZZ	Fracture fill ca	Calcite	21.7	− 5.3
SM08-11-B	WZZ	Scalenohedral ca fracture fill	Calcite	21.8	− 6.5
SM08-12-A	WZZ	Speleothem—interior radiating amber ca	Calcite	21.3	− 5.8
SM08-12-B	WZZ	Speleothem—white banded ca	Calcite	22.2	− 6.4
SM08-12-C	WZZ	Speleothem—5-mm colorless outer rind	Calcite	22.1	− 7.2
SM08-22-C	WZZ	5-mm ca on ss	Calcite	21.9	− 6.8
SM09-10-C	WZZ	ca-filled fracture	Calcite	21.4	− 6.6
SM-DD1	WZZ	Colorless ca in late fracture	Calcite	20.2	− 6.8
SMj-DD3	RZZ	Pore-fill ca mass	Calcite	21.9	− 8.5
EN1-2	RZZ	ca crystals	Calcite	20.5	− 3.9
SS11-2	RZZ	Massive pore-filling ca	Calcite	21.5	− 7.0
SM08-22 A	WZZ	Botryoidal bands	Smithsonite-type A	21.6	0.8
SM08-22 B	WZZ	Scalenohedral crust on mass ss	Smithsonite-type A	21.1	− 0.3
SM08-24	WZZ	Pendulous pale gray smithsonite	Smithsonite-type A	21.6	1.1
SM08-26	WZZ	White ss frc-fill and masses	Smithsonite-type A	21.5	− 0.2
SM03-07	WZZ	Multiple bands of white and colorless ss	Smithsonite-type B	22.1	1.0
SM03-09	WZZ	Dark gray and green ss	Smithsonite-type B	21.8	0.9
SM03-09-A	WZZ	Interior colloform dark gray green	Smithsonite-type B	21.9	0.6
SM03-09-B	WZZ	Exterior colloform white bands	Smithsonite-type B	21.4	− 0.8
SM03-27-A	WZZ	Colorless crystals	Smithsonite-type B	23.3	− 3.0
SM03-27-B	WZZ	Inner chalky band	Smithsonite-type B	21.4	− 5.1
SM03-27-C	WZZ	5-mm bluish band	Smithsonite-type B	22.3	− 1.9
SM03-27-D	WZZ	8-mm bluish band with minor white ss	Smithsonite-type B	22.3	− 1.8
SM08-06-2	WZZ	Outer 5-mm massive dark gray ss	Smithsonite-type B	22.3	− 1.8
SM08-06-3A	WZZ	Chalky ss	Smithsonite-type B	21.8	− 2.5
SM08-06-3B	WZZ	Interior of 5-mm smithsonite band	Smithsonite-type B	20.9	− 3.8
SM08-06-4A	WZZ	Exterior of 12- to 15-mm gray band	Smithsonite-type B	21.9	− 3.2
SM08-06-4B	WZZ	Interior of gray ss band	Smithsonite-type B	21.9	− 2.4
SM08-06-4C	WZZ	Exterior of gray ss band	Smithsonite-type B	21.6	− 2.4
SM08-06-5A	WZZ	Interior 8 mm of ~ 40-mm ss band	Smithsonite-Type B	22.0	− 1.4
SM08-06-5B	WZZ	8–16 mm zone	Smithsonite-type B	21.8	− 1.7
SM08-06-5C	WZZ	16–24 mm zone	Smithsonite-type B	21.7	− 2.1
SM08-06-5D	WZZ	24–32 mm zone	Smithsonite-type B	21.8	− 1.9
SM08-06-5E	WZZ	Exterior 8 mm of ~ 40-mm ss band	Smithsonite-type B	21.6	− 2.6
SM08-06-6	WZZ	Interior of 12- to 15-mm gray band	Smithsonite-type B	22.3	− 1.3
SM09-10-A	WZZ	Purple ss vug-fill crust	Smithsonite-type B	23.2	0.2
SM09-10-B	WZZ	Late green ss crust intergrown with Mn-ox	Smithsonite-type B	22.4	0.3
SM09-9-A	WZZ	Interior green yellow zone over Mn-ox	Smithsonite-type B	22.4	− 0.5
SM09-9-B	WZZ	Next 4-mm dark yellow green younger band	Smithsonite-type B	22.1	− 3.3
SM09-9-C	WZZ	Next 3-mm younger band	Smithsonite-type B	21.9	− 1.9
SM09-9-D	WZZ	Outermost 5-mm yellow band	Smithsonite-type B	22.1	− 1.6
SM08-10	WZZ	Pale purplish bands	Smithsonite-type B	21.8	− 8.4
SMj-PbC-1	PCM	Porous yellow-brown cerussite with silica bands and nodules to 5 mm	Cerussite	12.5	− 6.3

ca, calcite; *Mn-ox*, manganese oxides; *ss*, smithsonite; *PCM*, Lead Carbonate Manto; *RZZ*, Red Zinc Zone; *WZZ*, White Zinc Zone

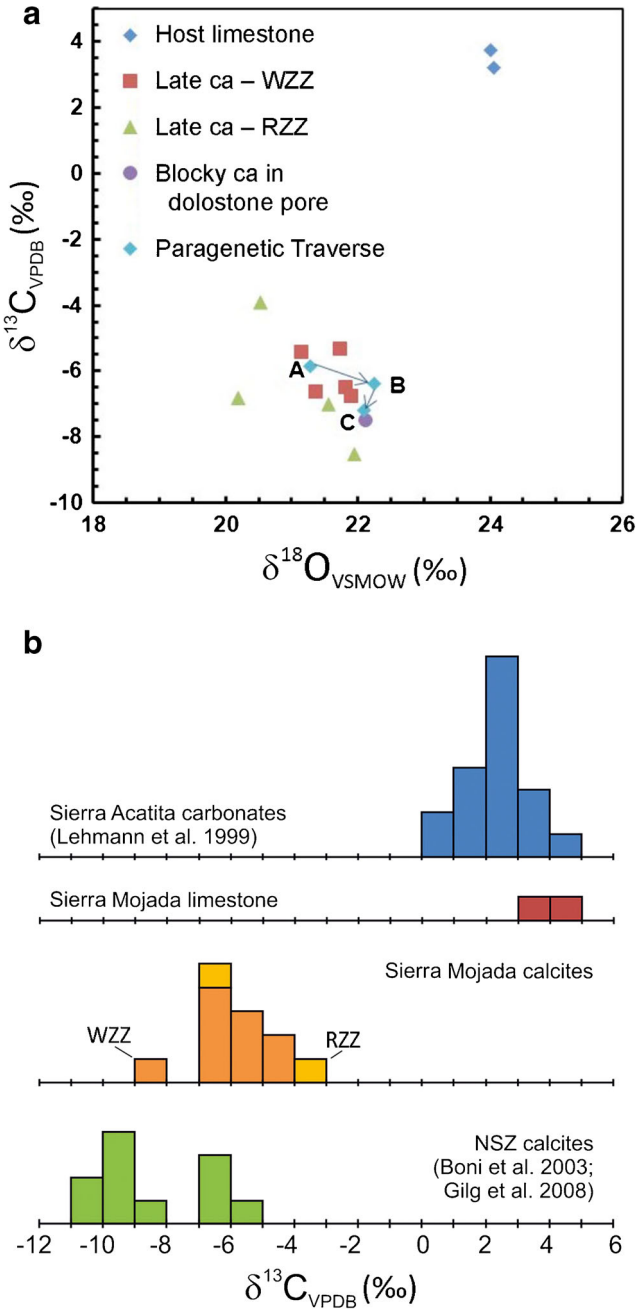

Fig. 12 Carbon and oxygen isotope composition of Sierra Mojada calcites. **a** Carbon and oxygen isotope values of calcite from the White Zinc Zone and the Red Zinc Zone and other Sierra Mojada calcites. **a**–**c** The isotope variations within a single sample from interior to rim. **b** Carbon isotope data of Sierra Mojada calcites compared to Coahuila Block Cretaceous carbonates (Lehmann et al. 1999) and to calcites associated with other NSZ deposits (Boni et al. 2003; Gilg et al. 2008)

from different paragenetic positions were analyzed (Table 2; Fig. 14). Bands from sample SM08-06 show a slight decrease of $\delta^{18}O$ values from 22.0 to 21.6‰ and a concomitant decrease of $\delta^{13}C$ values (−1.4 to −2.6‰) from early to late paragenetic stages. However, these isotopic trends are not consistent among other samples, and it is not possible to correlate smithsonite bands between samples.

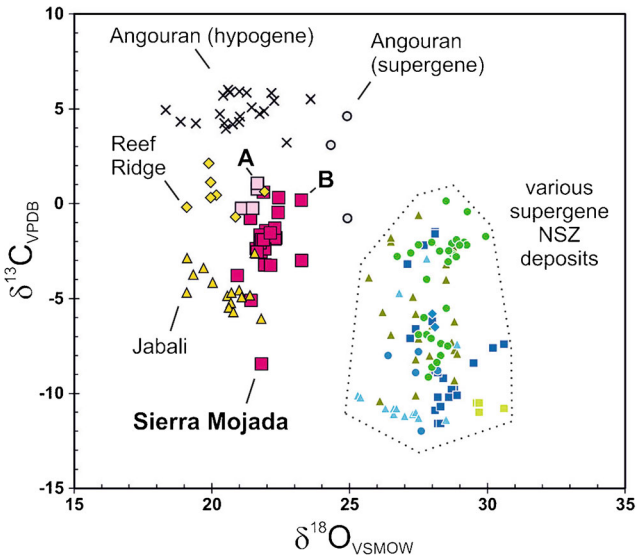

Fig. 13 Carbon and oxygen isotope values of Sierra Mojada smithsonite compared with other smithsonite deposits. Data sources for supergene smithsonites include Arfè et al. (2017), Boni and Mondillo (2015), Gilg et al. (2008), Mondillo et al. (2014), and Santoro et al. (2015). Data for hypogene and supergene smithsonites (Angouran, Iran) are from Boni et al. (2007)

A cerussite sample from the Lead Carbonate Manto has a $\delta^{18}O$ value of 12.5‰ (Table 2), ~ 10 ‰ lower than smithsonites reported for most supergene NSZ ores, consistent with smithsonite-cerussite oxygen isotope fractionation below 40 °C (Gilg et al. 2008). The carbon isotope composition of the cerussite is relatively low (− 6.3‰).

Lead isotopes of lead and zinc minerals

The Pb isotope composition of galena, cerussite, smithsonite, and hemimorphite was measured to evaluate genetic relations among the sulfide and nonsulfide orebodies (Table 3). Sierra

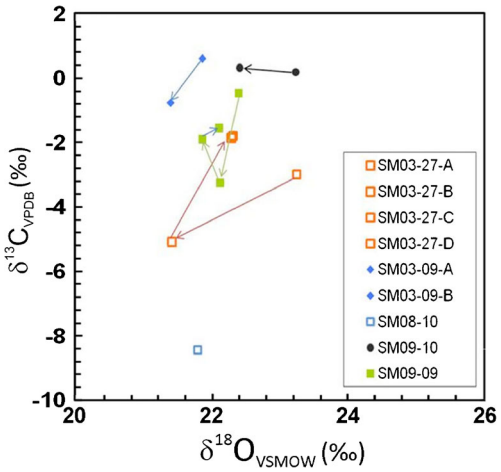

Fig. 14 Carbon and oxygen isotope variation of Sierra Mojada smithsonite-B by paragenetic position. Arrows indicate younging paragenetic position

Table 3 Lead isotope compositions of Sierra Mojada galena and secondary Pb and Zn minerals

Sample	Ore zone	Description	Mineral	$^{206}Pb/^{204}Pb$	$^{207}Pb/^{204}Pb$	$^{208}Pb/^{204}Pb$
SM03-4	Veta Rica	Galena stringers in coarse-crystalline barite	Galena	18.676	15.638	38.551
SM08-Pb01	Veta Rica	Massive fine-grained galena	Galena	18.697	15.648	38.575
SM-S3-Pb	Polymetallic zone	Coarse galena in dolostone	Galena	18.693	15.642	38.559
D7080226–25.5	Polymetallic zone	Polymetallic sulfides in dolostone breccia	Galena	18.687	15.636	38.534
D9090317–13	Polymetallic zone?	Galena remnants in oxidized fracture in dolostone	Galena	18.634	15.631	38.495
DRMT08–1	Dormitos prospect	cm cubic galena crystal in dolostone	Galena	18.691	15.650	38.593
DRMT08–2	Dormitos prospect	cm cubic galena crystal in dolostone	Galena	18.700	15.662	38.633
SMj-PbC-1	Lead Carbonate Manto	Porous yellow-brown cerussite with silica bands and nodules to 5 mm	Cerussite	18.692	15.647	38.575
SM03–09	White Zinc Zone	Colloform dark gray and green smithsonite B	Smithsonite	18.697	15.637	38.536
SM09–9	White Zinc Zone	1.5-cm green yellow colloform smithsonite	Smithsonite	18.847	15.629	38.482
WZ06–5	White Zinc Zone	10-cm colloform smithsonite	Smithsonite	18.693	15.635	38.532
EN1–3	Red Zinc Zone	Hemimorphite crystals in tabular pores in iron oxide matrix	Hemimorphite	18.680	15.627	38.512

Mojada galena samples ($n = 7$) have $^{206}Pb/^{204}Pb$ ratios between 18.634 and 18.700 (average = 18.679), $^{207}Pb/^{204}Pb$ between 15.631 and 15.662 (average = 15.644), and $^{208}Pb/^{204}Pb$ between 38.495 and 38.633 (average = 38.563). The galena samples represent a variety of district occurrences and ore types from polymetallic sulfide deposits to remnant galena in oxidized ores. The Pb isotope compositions of cerussite, smithsonite, and hemimorphite are similar to that of galena (Fig. 15), except for one galena sample distal to the main mineralized zone that may represent a different mineralization type or stage.

Interpretation and discussion

Hypogene mineralization

The deeply weathered character of the Sierra Mojada District ores has created a less than ideal situation to constrain the nature and origin of the hypogene metal concentrations that were precursor to the supergene mineralization. Two primary mineralization types have been suggested: (1) a polymetallic carbonate-replacement (CRD) system of the type present elsewhere in northern Mexico (Megaw et al. 1988, 1996) and (2) a sedimentary basinal brine system (MVT) (Tritlla et al. 2007; González-Sánchez et al. 2009).

Both CRD and MVT ore systems show a range of relative Zn and Pb concentrations. However, MVT systems seldom have significant Ag and Cu contents that are more typical of CRD systems, although some sedimentary basin ore systems have appreciable Ag ± Cu (e.g., Goodfellow et al. 1993; Kyle and Saunders 1996). In either case, the fundamental question of whether CRD mineralization may involve both magmatic and sedimentary brines (Megaw et al. 1996; Kyle 2012) is not answered by current information on Sierra Mojada.

As calc-silicate minerals have not been reported in the Sierra Mojada District, it appears that the mineralizing fluids were not of the higher temperature and appropriate chemical character to cause development of skarns in the host carbonate sequence (e.g., Gilg 1996). Thus, Sierra Mojada mineralization-related alteration is subtle, consisting principally of hydrothermal ferroan dolomite and microcrystalline silica that are typical of distal CRD alteration.

Associated sphalerite-galena reveals a $\Delta^{34}S$ value of 3.1‰, suggesting an equilibration temperature of ~200 °C, similar to calculated temperatures for a barite-galena pair (Table 1). Thus, the overall information based on alteration styles and sulfur isotope fractionation suggests the Sierra Mojada primary mineralization resulted from circa 200 °C fluids. The bimodal nature of the sulfide sulfur isotope data, as well as associated barite having values similar to Albian evaporites (Table 1), suggests an involvement of sedimentary sulfur in the primary mineralization system, as has been suggested for other CRD systems (cf. Megaw 1990; Gilg 1996).

The Pb isotope composition of the Sierra Mojada mineralization is similar to mid-Cenozoic CRD in northern Mexico at Naica (James and Henry 1993) and at nearby Mapimi, Durango (Kyle, unpubl. data) (Fig. 1). However, these data are more radiogenic than the carbonate replacement and skarn deposits at Santa Eulalia, Dos Marias, and San Carlos (James and Henry 1993) (Fig. 15). However, the Pb isotope character of all northern Mexico CRD is distinctly different from the Laramide porphyry Cu-Mo-associated CRD at Shafter in contiguous Texas (James and Henry 1993; Gilmer et al. 2003), suggesting a genetic affiliation among the mid-Cenozoic CRD.

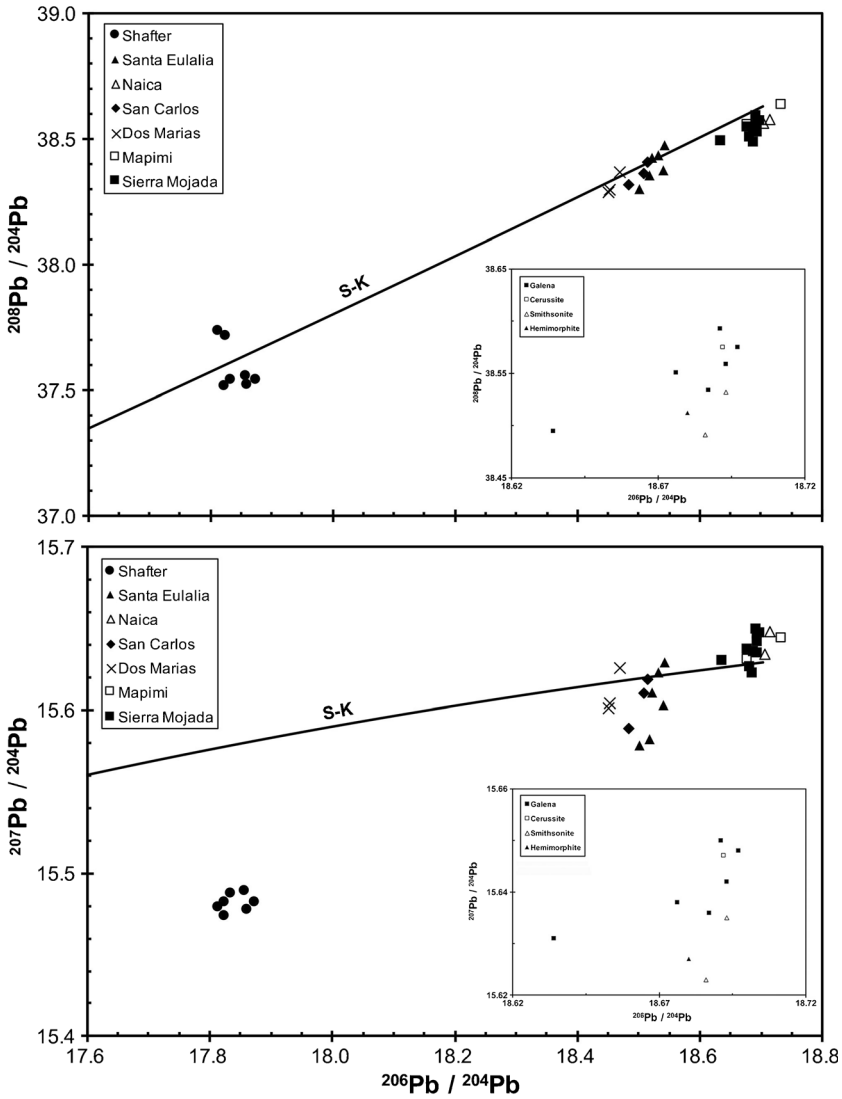

Fig. 15 Plot of Pb isotopes for Pb-bearing minerals in the Sierra Mojada District, compared to other polymetallic carbonate replacement deposits in north central Mexico and adjacent Texas. Expanded inset plots show Sierra Mojada Pb isotope compositions by mineral (Table 3). S-K Stacey and Kramers (1975) growth curve. Data from James and Henry (1993) and this study

Supergene mineralization

The NSZ concentrations at Sierra Mojada are similar to the "red zinc" and "white zinc" deposits described for many supergene deposits worldwide (Hitzman et al. 2003). Smithsonite from Sierra Mojada is generally similar to those described elsewhere with similar mineral habits, as described in Sardinia (Boni et al. 2003) and the Irish Midlands (Balassone et al. 2008).

The similarity of Pb isotope ratios of smithsonite from the White Zinc Zone, hemimorphite from the Red Zinc Zone, and cerussite from the Lead Carbonate Manto to the Pb isotopic ratios of the Sierra Mojada hypogene galena samples (Table 3; Fig. 15) confirms that the source of the metals present in the NSZ deposits was the polymetallic carbonate-replacement sulfide mineralization.

Compared to C-O isotope values of Cretaceous marine carbonates (averages of 27.7 and 2.4‰ for $\delta^{18}O_{VSMOW}$ and $\delta^{13}C_{VPDB}$, respectively; Veizer and Hoefs 1976), the carbon isotope values of limestone in the Sierra Mojada District are slightly higher, and oxygen isotope values are slightly lower (Fig. 12b). These stable isotope values can be compared to Aptian through Albian interbedded carbonates and evaporites of the Acatita Formation at Sierra Acatita ~ 100 km southeast of Sierra Mojada on the Coahuila Block (Lehmann et al. 1999). The $\delta^{13}C$ values of the Sierra Mojada limestones are within the range of carbonates from the Sierra Acatita. Most of the carbon isotope compositions of late calcite in the Sierra Mojada District are slightly heavier, whereas oxygen isotope values are lower than those of other NSZ deposits (Boni et al. 2003; Coppola et al. 2008).

The isotope composition of Sierra Mojada smithsonites shows a relatively wide range for the carbon and restricted values for oxygen that is characteristic for most supergene NSZ deposits (Boni et al. 2003, 2007; Gilg et al. 2008; Coppola et al. 2008; Mondillo et al. 2014; Santoro et al.

2015; Boni and Mondillo 2015). Only a few carbonate-hosted supergene smithsonite deposits have a restricted carbon isotope range, such as Vila Ruiva, Portugal (Gilg et al. 2008), and the Red Galman ores in the Silesian deposits, Poland (Coppola et al. 2009), both of which are dominated by isotopically light carbon. Hypogene, travertine-associated Zn carbonates at the Angouran deposit, Iran, show a large range of oxygen isotope values related to variable temperatures and have unusually high and constant $\delta^{13}C$ values characteristic of contact-metamorphic CO_2 (Boni et al. 2007).

The large spread of $\delta^{13}C$ values of Sierra Mojada smithsonite is similar to that of many other supergene carbonate-hosted smithsonites, suggesting at least two distinct carbon sources. A ^{13}C-depleted source could be related to organic matter decomposition from overlying soils, oxidation by sulfide-oxidizing bacteria in sulfide bodies as a result of a lowering water table, or organic carbon-rich wall rocks. The ^{13}C-enriched carbonate is either derived from the host marine carbonates, from atmospheric CO_2, or derived from C4-plant dominated soils (Gilg et al. 2008). Hydrothermal gangue carbonates related to the primary sulfide mineralization may be an additional isotopically variable source of carbon.

In the White Zinc Zone, the early smithsonite-A is dominated by a relatively heavy carbon source, most likely hydrothermally altered Cretaceous marine host carbonates, whereas the later stage smithsonite-B shows a large carbon isotope range indicating variable carbon sources. High Mn contents in CL-luminescent ^{13}C-depleted smithsonite are an indicator of more reducing conditions, consistent with interaction with organic carbon during the late mineralization stage. Late pore-filling calcite that postdates NSZ mineralization has low carbon isotope values indicating a significant shift in the carbon source during crystallization from Zn to Ca carbonates.

As organic carbon-rich Cretaceous sediments are absent in the vicinity of White Zinc Zone, the ^{13}C-depleted carbon is most probably related to soil carbon in the fluid recharge area. The present flora of the Sierra Mojada region is dominated by members of Yucca family, including the palms and lechuguilla (*Agave lechuguilla*) and various cacti (Riley 1936) that are CAM (crassulacean acid metabolism) species. Mesquite, a C3 plant, is present but is relatively uncommon.

C3 grasses generally have lower $\delta^{13}C$ values (average − 26‰) than C4 grasses (average − 12‰), whereas CAM plants commonly are between these values (Cerling 1984; Cerling and Quade 1993). The carbon isotope values of late-stage calcites in the NSZ ores are thus consistent with a derivation from predominantly CAM plants, perhaps with some admixture of C3 and C4 plant carbon. This would be similar to pedogenic cabonates in other arid areas of northern Mexico (Cruz-Y-Cruz et al. 2015) and Texas (Zhou and Chavez 2010). However, the climate of northern Mexico has changed markedly in the Pleistocene (Metcalfe et al. 2000). Given that the Sierra Mojada supergene NSZ system appears to be no longer active, it is likely that surface plant assemblages during active NSZ mineralization would have been different from those in the modern arid climate.

The $\delta^{18}O$ values of Sierra Mojada smithsonite are much lower than those reported in most supergene NSZ deposits, which generally range from 26 to 31‰ (Gilg et al. 2008; Boni and Mondillo 2015; Fig. 13). Only two other supergene deposits investigated so far have similarly low oxygen isotope values for smithsonite, the Reef Ridge prospect, Alaska (Santoro et al. 2015), and the Jabali deposit, Yemen (Mondillo et al. 2014). While strongly ^{18}O-depleted waters (− 15‰) and low temperatures of sulfide oxidation of about 10 °C are suggested for the high-latitude Alaskan prospect (Santoro et al. 2015), moderately high temperatures are suggested for the Yemeni deposit (Mondillo et al. 2014).

Formational temperatures of smithsonite from Sierra Mojada can be constrained by oxygen isotope equilibrium between smithsonite and water (Gilg et al. 2008) if the $\delta^{18}O$ value of paleometeoric water is known. Although the paleometeoric water $\delta^{18}O$ value is unavailable for the Sierra Mojada District, modern groundwater in the region can be used to estimate the $\delta^{18}O$ water value. If the Sierra Mojada paleometeoric water had a similar oxygen isotope composition as modern high elevation groundwaters at Cuatrociénegas, Coahuila (150 km east of Sierra Mojada) (Johannesson et al. 2004; Wassenaar et al. 2009; Wolaver et al. 2013) and as modern precipitation that is recharged at an elevation of about 1400 to 1500 m, then, a $\delta^{18}O_{VSMOW}$ value of about − 8‰ is estimated for the Sierra Mojada NSZ-mineralizing waters. Using this isotopic composition for water, formational temperatures for smithsonite and calcite can be calculated using the oxygen isotope fractionation for smithsonite (Gilg et al. 2008) and calcite (O'Neil et al. 1969), respectively.

The calculated equilibrium temperature is 35 °C for cerussite, 34 ± 1 °C for smithsonite-A, and 31 ± 2 °C for smithsonite-B. Modern spring discharge temperatures at Cuatrociénegas are as high as 35 °C (Wolaver et al. 2013); thus, moderately elevated temperatures for smithsonite precipitation are not unreasonable for this extensional tectonic terrane. Using the same $\delta^{18}O$ value for water, equilibration temperatures for late calcite are calculated to be 14 to 19 °C in the White Zinc Zone and 15 to 23 °C in the Red Zinc Zone, suggesting a lower temperature post-NSZ mineralization groundwater system was responsible for late pore-filling calcite (Supplemental Materials 2). Alternatively, if temperature was constant, then an increase of the $\delta^{18}O$ value of the waters is required.

If the recharge area for the early sulfide oxidation water was located at a higher average elevation, then the $\delta^{18}O$ value of this water can be estimated at about − 10‰ using the regional altitude effect for oxygen isotope composition of precipitation (Rodríguez et al. 2005). With such a lower oxygen

isotope value for the oxidation water, the formation temperatures are ~ 25 °C for smithsonite-A, 22 ± 5 °C for smithsonite-B, and 23 °C for cerussite. Even in this scenario of a water oxygen isotope increase due to a change in the elevation of the recharge area, a slight temperature decrease from early smithsonite to late calcite is indicated. We interpret this temperature and possibly also the isotope compositional change of the ground waters to a rearrangement of groundwater flow and a time gap between early sulfide oxidation and late calcite precipitation, probably in the Pleistocene. These changes are also accompanied by a decrease of carbon isotope values from early smithsonite to late calcite. Overall, the unusually low oxygen isotope values of smithsonites at Sierra Mojada are considered a combination of high elevation-recharged ground waters and moderate temperatures of sulfide oxidation.

Geochemical controls of supergene Pb and Zn mineralization are discussed by many authors including Takahashi (1960), Sangameshwar and Barnes (1983), Williams (1990), and Reichert and Borg (2008). The oxidation of pyrite and Fe-bearing sphalerite and the precipitation of Fe hydroxides are important factors in the development of NSZ mineralization because these processes lower the groundwater pH locally. The released acids can transport metals and react with wall rock carbonates causing the constant consumption of H^+. The released carbonate species may react with metal ions and precipitate secondary minerals. Thus, Fe-rich sulfide replacements (so-called red ores) may have different geochemical precipitation conditions and mineral compositions from carbonate wall rock replacements ("white ores") (Reichert and Borg 2008).

High P CO_2(g) increases the stability of smithsonite due to the increased activity of HCO_3^-(aq) and CO_3^{2-} (aq) in the aqueous fluids. A minimum P CO_2(g) of 0.4 kPa is required for smithsonite precipitation, which is higher than atmospheric or arid soil P CO_2(g) (Reichert and Borg 2008). If P CO_2(g) is greater than 0.4 kPa, smithsonite precipitation will be favored instead of hydrozincite (Reichert and Borg 2008). In the unsaturated zone, with greater communication with the atmosphere, hydrozincite would be more stable than smithsonite because the stability of smithsonite requires higher P CO_2 than atmospheric CO_2 or P CO_2 (Fig. 16). Because smithsonite is the least soluble NSZ mineral at 25 °C and neutral conditions, typical of weathering environments, it is the most abundant mineral in supergene NSZ deposits (Hitzman et al. 2003). The abundance of smithsonite in the White Zinc Zone of the Sierra Mojada deposit with high carbon isotope values in early (A) and most late-stage smithsonite (B) thus corresponds to wall rock replacements or "white ores" where most of the carbon is derived from the wall rocks. In the waning stages of Zn carbonate mineralization and during calcite deposition, soil-derived organic carbon becomes a more prominent source.

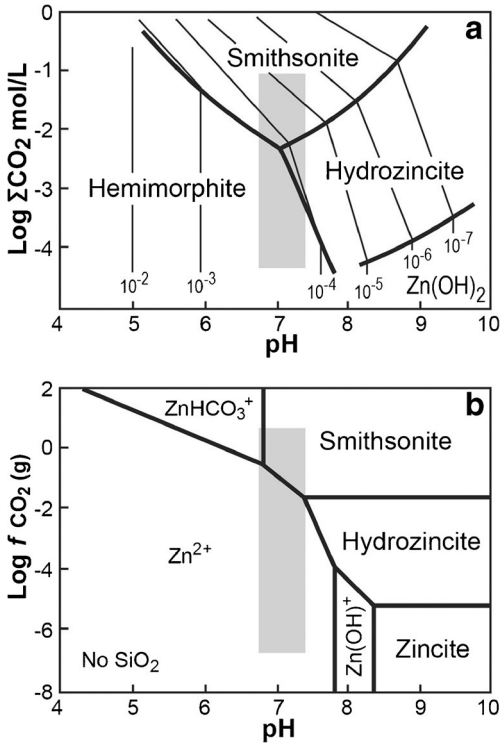

Fig. 16 Stability fields of nonsulfide Zn minerals. **a** Possible maximum stability field of hemimorphite in silica-saturated solutions at 25 °C. Contour lines indicating Zn mol/L in solution. After Takahashi (1960). **b** Stabilities of Zn minerals with "Zn species" = 10^{-5} and atmospheric CO_2 of $10^{-3.5}$, with the absence of silica. After McPhail et al. (2003). Shaded area indicates the pH range of modern Sierra Mojada area groundwater

Hemimorphite commonly forms from the oxidation of sphalerite when silica is present under acidic to slightly alkaline pH conditions (Fig. 16a). The stability fields of hemimorphite and hydrozincite can be changed by different P CO_2(g) values and the chemistry of mineral assemblages in equilibrium with aqueous fluids (Reichert and Borg 2008). Hydrozincite and smithsonite are less stable under acidic conditions than hemimorphite (Fig. 16b). If the solution is undersaturated with silica, hemimorphite stability is constrained to a more acidic field (Takahashi 1960). Sauconite would be more stable under more alkaline pH conditions (McPhail et al. 2003, 2006). An increase in silica activity and a decrease of CO_2 activity at near neutral pH conditions favor hemimorphite precipitation, while high CO_2 is necessary for smithsonite crystallization. Hydrozincite in contrast requires slightly lower CO_2 activities and higher pH.

Meteoric waters appear to be responsible for precipitation of NSZ minerals in an evolving groundwater system at Sierra Mojada. The oxygen isotope values of smithsonite at Sierra Mojada are slightly lower than that of most supergene smithsonites (Fig. 13) suggesting that the formational temperature for some Sierra Mojada smithsonite could be as high as 35 °C. These somewhat elevated groundwater temperatures could be related to the regional tectonic structure of northern Mexico

with an active extensional province accounting for a high geothermal gradient. Lower temperatures were calculated for late calcite associated with smithsonite and hemimorphite, which may indicate temperature changes to the groundwater system after NSZ mineralization had ceased locally.

Regional climate relationships

NSZ mineralization at Sierra Mojada resulted from precipitation of Zn from groundwater that redistributed significant amounts of Zn and other metals derived from the oxidation of primary sulfide deposits. The timing for the onset of sulfide oxidation and formation of supergene NSZ deposits is not well constrained, but the system could have developed in the late Cenozoic. Stephenson et al. (2014) documented uplift rates of 0.15 to 0.2 mm/year for this region from 25 to 8 Ma, followed by a period of relative crustal stability. In comparison with other polymetallic carbonate-replacement deposits in northern Mexico (e.g., Megaw et al. 1988), Sierra Mojada hypogene mineralization would have been emplaced during the mid-Cenozoic, thus predating regional uplift. Even the lower rates imply ample time to uplift and unroof the Sierra Mojada hypogene mineralized zone by removing the younger Cretaceous succession (Fig. 3), even if thickened by Laramide deformation, as well as at least 1 km of mid-Cenozoic ignimbrites. The precise initial exposure of Sierra Mojada hypogene sulfide mineralization to oxidizing groundwater cannot be constrained further with present information.

Although there have been no local studies, climatic conditions in northern Mexico in the Late Pleistocene and early Holocene have been documented to have been generally cooler and wetter than the Present (Metcalfe et al. 2000). There is evidence for the presence of Pleistocene lakes in what is now the modern Chihuahuan desert, including the remnant salt flat at Laguna del Rey ~ 40 km southeast of Sierra Mojada (Sanchez-Mejorada 1987). The abundance of sauconite at Sierra Mojada may be related to the arid climate as the formation of sauconite from aluminosilicates is facilitated by relatively closed alkaline environments as suggested by Boni et al. (2009) and Mondillo et al. (2015).

Transition to the modern desert climate probably began in north central Mexico around 12,000 years BP and became established about 9000 years BP (Metcalfe et al. 2000). This transition would have been complicated by Younger Dryas global events. Arid conditions, at least seasonally, have been modeled to be more favorable for NSZ mineralization (Reichert and Borg 2008). Transition to and stabilization of the modern desert climate in the Sierra Mojada region over the past 9000 years would have resulted in episodic drawdown of the water table and termination of local supergene metal mobilization, thus preserving the NSZ deposits.

Conclusions

The similarity of the Pb isotope composition of smithsonite, hemimorphite, and cerussite to that of galena samples and other geological relationships indicates that polymetallic carbonate-replacement sulfide deposits were the likely source of metals in Sierra Mojada NSZ mineralization. The redistribution of Zn and other metals from the primary sulfide concentrations was influenced by topography-controlled groundwater flow focused by local structural features that resulted in different types of secondary mineralization. The dynamic nature of the groundwater systems is confirmed by the coarse-laminated sediments within the paleo-dissolution structures. Smithsonite is locally replaced and crosscut by hemimorphite, but also can be locally intergrown with hydrozincite, as well as hemimorphite-A and sauconite. Hemimorphite-A has replaced, or intergrown with, smithsonite, whereas tabular hemimorphite (hemimorphite-B) displays pore-filling features locally crosscutting smithsonite. These relationships suggest an evolving system with alternating water chemistry near the intersection of the stability fields of these minerals (Fig. 16). Equilibrium fractionation modeling based on local and regional groundwater $\delta^{18}O$ data suggest that some smithsonite was precipitated at temperatures of circa 35 °C. Although the timing of NSZ mineralization is not well constrained, the abundance of late-stage, post-NSZ mineralization calcite in the NSZ ore zones and their $\delta^{18}O$ values indicate precipitation from lower temperature groundwater, signifying termination of the local conditions responsible for NSZ formation.

The fluids that deposited the high concentrations of hemimorphite contained significant aqueous silica that was most likely sourced from biogenic silica in the Cretaceous wall rocks and in microcrystalline silica in the polymetallic ores. The abundance of hemimorphite indicates silica was mobile during supergene alteration. Weakly acidic fluids generated from sulfide oxidation and buffered by silica-rich carbonate host rocks would have favored hemimorphite precipitation. Depletion of local silica sources and/or increasing pH conditions by wall rock buffering likely resulted in smithsonite-dominant, with local hydrozincite, mineralization. Although the timing of NSZ mineralization is not well constrained, the position of the modern groundwater table well below the level of the NSZ ore zones, as well as late-stage pore-filling calcites, suggests that supergene NSZ mineralization is a product of an older groundwater system that was terminated due to a lowered water table during the transition from the wetter, cooler Late Pleistocene climate to the modern arid climate.

Acknowledgements We are grateful to Metalline Mining Company, specifically to the late Dr. Roger Kolvoord, for providing initial access and permission to conduct research on the Sierra Mojada District. We thank Dr. N. Miller and Dr. L. Mack at the Jackson School of Geosciences for

providing assistance with LA-ICP-MS trace element analysis of smithsonite and Pb isotope analysis of Pb and Zn minerals, respectively, and Dr. U. Struck for stable isotope measurements of carbonates at the Museum für Naturkunde, Berlin, Germany. Review of portions of an earlier version of the manuscript by Dr. S. Loewy and Dr. B. Wolaver, as well as critiques of the submitted manuscript by two anonymous reviewers and the editors, improved the clarity of presentation.

Funding information Funding for research support was provided by Metalline Mining Company, a student research grant from the Society of Economic Geologists, and the C. E. Yager Professorship and other funds from Geology Foundation of the Jackson School of Geosciences.

References

Ahn, H (2010) Mineralogy and geochemistry of the non-sulfide zinc deposits in the Sierra Mojada District, Coahuila, Mexico. MS thesis, Univ Texas Austin (179 p)

AKF Mining Services (2015) Updated NI43-101 technical report on the resources of the Sierra Mojada project, Coahuila, Mexico: Report prepared for Silver Bull Resources (205 p) http://www.silverbullresources.com/i/pdf/reports/NI43-101-Technical-Report.pdf

Arfè G, Boni M, Balassone G, Mondillo N, Hinder G, Joachimski M (2017) New C–O isotopic data on supergene minerals from the Skorpion and Rosh Pinah ore deposits (Namibia): genetic and paleoclimatic constraints. J Afr Earth Sci 126:148–158

Balassone G, Rossi M, Boni M, Stanley G, McDermott P (2008) Mineralogical and geochemical characterization of nonsulfide Zn-Pb mineralization at Silvermines and Galmoy (Irish Midlands). Ore Geol Rev 33:168–186

Boni M, Balassone G, Arseneau V, Schmidt P (2009) The nonsulfide zinc deposit at Accha (southern Peru): geological and mineralogical characterization. Econ Geol 104:267–289

Boni M, Gilg HA, Aversa G, Balassone G (2003) The "calamine" of southwest Sardinia: geology, mineralogy, and stable isotope geochemistry of supergene Zn mineralization. Econ Geol 98:731–748

Boni M, Gilg HA, Balassone G, Schneider J, Allen C, Moore F (2007) Hypogene Zn carbonate ores in the Angouran deposit, NW Iran. Mineral Deposita 42:799–820

Boni M, Mondillo N (2015) The "Calamines" and the "Others": the great family of supergene nonsulfide zinc ores. Ore Geol Rev 67:208–233

Buatier M, Choulet F, Petit S, Chassagnon R, Vennemann T (2016) Nature and origin of natural Zn clay minerals from the Bou Arhous Zn ore deposit: evidence from electron microscopy (SEM-TEM) and stable isotope compositions (H and O). Appl Clay Sci 132:377–390

Campa MF, Coney PJ (1983) Tectono-stratigraphic terranes and mineral resource distributions in Mexico. Can J Earth Sci 20:1040–1051

Cerling TE (1984) The stable isotopic composition of modern soil carbonate and its relationship to climate. Earth Planet Sci Lett 71:229–240

Cerling TE, Quade J (1993) Stable carbon and oxygen isotopes in soil carbonates. Geophys Monogr 78:217–231

Chávez-Cabello G, Aranda-Gomez JJ, Molina-Garza RS, Cossío-Torres T, Arvizu-Gutiérrez IR, González-Naranjo GA (2007) The San Marcos fault: a Jurassic multireactivated basement structure in northeastern Mexico. Geol Soc Am Spec Pap 422:261–286

Choulet F, Buatier M, Barbanson L, Guégan R, Ennaciri A (2016) Zinc-rich clays in supergene non-sulfide zinc deposits. Mineral Deposita 51:467–490

Coppola V, Boni M, Gilg HA, Balassone G, Dejonghe L (2008) The "calamine" nonsulfide Zn–Pb deposits of Belgium: petrographical, mineralogical and geochemical characterization. Ore Geol Rev 33: 187–210

Coppola V, Boni M, Gilg HA, Strzelska-Smakowska B (2009) Nonsulfide zinc deposits in the Silesia–Cracow district, Southern Poland. Mineral Deposita 44:559–580

Cruz-y-Cruz T, Sedov S, Sánchez G, Pi-Puig T, Pustovoytov K, Barceinas-Cruz H, Ortega-Guerrero B, Solleiro-Rebolledo E (2015) Late Pleistocene - Holocene paleosols in the north of Sonora, Mexico: chronostratigraphy, pedogenesis and implications for environmental history. Eur J Soil Sci 65:455–469

De Wet JR, Singleton JD (2008) Development of a viable process for the recovery of zinc from oxide ores. J South Afr Inst Min Metall 108: 253–259

Gilg HA (1996) Fluid inclusion and isotope constraints on the genesis of high-temperature carbonate-hosted Pb-Zn-Ag deposits. In: Sangster D (ed) Carbonate-hosted lead zinc deposits: Society of Economic Geologists Special Publication 4, pp 501–514

Gilg HA, Boni M, Hochleitner R, Struck U (2008) Stable isotope geochemistry of carbonate minerals in supergene oxidation zones of Zn-Pb deposits. Ore Geol Rev 33:117–133

Gilg HA, Struck U, Vennemann T, Boni M (2003) Phosphoric acid fractionation factors for smithsonite and cerussite between 25 and 72°. Geochim Cosmochim Acta 67:4049–4055

Gilmer AK, Kyle JR, Connelly JN, Mathur RD, Henry CD (2003) Extension of Laramide magmatism in southwestern North America into Trans-Pecos Texas. Geology 31:447–450

Goldhammer RK (1991) Sequence stratigraphy and cyclostratigraphy of the Mesozoic of the Sierra Madre Oriental, northeast Mexico: a field guidebook. Society of Economic Paleontologists and Mineralogists Foundation, Gulf Coast Section (65 p)

González-Sánchez F, Camprubí A, González-Partida E, Puente-Solís R, Canet C, Centeno-García E, Atudorei V (2009) Regional stratigraphy and distribution of epigenetic stratabound celestine, fluorite, barite and Pb–Zn deposits in the MVT province of northeastern Mexico. Mineral Deposita 44:343–361

Goodfellow WD, Lydon JW, Turner RJW (1993) Geology and genesis of stratiform sediment-hosted (SEDEX) zinc-lead-silver sulphide deposits. In: Kirkham RV, Sinclair WD, Thorp RI, Duke JM (eds) Mineral Deposit Modeling: Geological Association of Canada Special Paper 40, pp 201–251

Götte T, Richter DK (2004) Quantitative high-resolution cathodoluminescence spectroscopy of smithsonite. Mineral Mag 68:199–207

Gryger, SM (2010) Geologic framework of the Sierra Mojada mining district, Coahuila, Mexico: an integrative study of a Mesozoic platform-basin margin. MS thesis, Univ Texas Austin (376 p)

Hitzman MW, Reynolds NA, Sangster DF, Allen CR, Carman CE (2003) Classification, genesis, and exploration guides for nonsulfide zinc deposits. Econ Geol 98:685–714

Hodder RW (2001) Carbonate-hosted zinc deposits, Sierra Mojada district, State of Coahuila, Mexico; a review of potential: internal Metalline Mining Company report (66 p)

James EW, Henry CD (1993) Southeastern extent of the North American craton in Texas and northern Chihuahua as revealed by Pb isotopes. Geol Soc Am Bull 105:116–126

Johannesson KH, Cort A, Kilroy KC (2004) Reconnaissance isotopic and hydrochemical study of Cuatro Ciénegas groundwater, Coahuila, Mexico. J S Am Earth Sci 17:171–180

Kyle JR (2012) Sierra Mojada Ag-Pb-Zn District, Coahuila: an endmember carbonate replacement mineralization system? Geological Society of America, Cordilleran Section Abstracts with Programs 44:72

Kyle JR, Saunders JA (1996) Metallic deposits in the Gulf Coast Basin of southern North America: diverse mineralization styles in a young sedimentary basin. In: Sangster D (ed) Carbonate-hosted lead zinc

deposits: Society of Economic Geologists Special Publication 4, pp 218–229

Lehmann C, Osleger DA, Montanez IP, Sliter W, Vanneau AA, Banner J (1999) Evolution of Cupido and Coahuila carbonate platforms, Early Cretaceous, northeastern Mexico. Geol Soc Am Bull 111: 1010–1029

Luhr JF, Aranda-Gómez JJ, Housh TB (1995) San Quintín volcanic field, Baja California Norte, Mexico: geology, petrology, and geochemistry. J Geophys Res 100(B7):10353–10380

McPhail DC, Summerhayes E, Jayaratne V, Christy A (2006) Hemimorphite solubility and stability of low-T zinc minerals. Geochim Cosmochim Acta 70:A414–A414

McPhail DC, Summerhayes E, Welch S, Brugger J (2003) The geochemistry and mobility of zinc in the regolith: Cooperative Research Centre for Landscape Environments and Mineral Exploration, Proceedings of the CRC LEME Regional Regolith Symposia, Western Australia, pp 287–291

Megaw PKM (1990) Geology and geochemistry of the Santa Eulalia mining district, Chihuahua, Mexico: unpublished Ph.D. dissertation, Univ. Arizona (549p)

Megaw PKM (2009) Evaluation of oxidized Pb-Zn-Ag carbonate replacement deposits of Mexico in light of supergene zinc and residual lead enrichment processes. In: Titley SR (ed) Supergene environments, processes, and products: Society of Economic Geologists Special Publication 14, pp 51–59

Megaw PKM (2010) Geology and genesis of (most) collectible smithsonite. In: Hughes T, Liebetrau S, Staebler G (eds) Smithsonite: think zinc! Lithographie, Denver, 18–24

Megaw PKM, Barton MD, Falce FI (1996) Carbonate-hosted lead zinc (Ag, Cu, Au) deposits of northern Chihuahua, Mexico. In: Sangster D (ed) Carbonate-hosted lead zinc deposits: Society of Economic Geologists Special Publication 4, pp 277–289

Megaw PKM, Ruiz J, Titley SR (1988) High-temperature, carbonate-hosted Ag-Pb-Zn(Cu) deposits of northern Mexico. Econ Geol 83: 1856–1885

Metcalfe SE, O'Hara SL, Caballero M, Davies SJ (2000) Records of Late Pleistocene–Holocene climatic change in Mexico—a review. Quat Sci Rev 19:699–721

Mondillo N, Boni M, Balassone G, Joachimski M, Mormone A (2014) The Jabali nonsulfide Zn–Pb–Ag deposit, western Yemen. Ore Geol Rev 61:248–267

Mondillo N, Nieto F, Balassone G (2015) Micro-and nano-characterization of Zn-clays in nonsulfide supergene ores of southern Peru. Am Mineral 100:2484–2496

O'Neil JR, Clayton RN, Mayeda T (1969) Oxygen isotope fractionation in divalent metal carbonates. J Chem Phys 51:5547–5558

Ohmoto H, Goldhaber MB (1997) Sulfur and carbon isotopes. In: Barnes HL (ed) Geochemistry of hydrothermal ore deposits: J Wiley and Sons, pp 517–611

Reichert J, Borg G (2008) Numerical simulation and a geochemical model of supergene carbonate-hosted non-sulphide zinc deposits. Ore Geol Rev 33:134–151

Riley LB (1936) Geology and ore deposits of Sierra Mojada, Coahuila, Mexico. PhD dissertation, Yale University (343 p)

Rodríguez AAA, Mijares FJA, Ojeda CG, Morales MM, Hita LG, Zamarrón GH, Arellano IM, González MAM, Flores GO, Almanza PG, Sánchez RL, López JLP, Arzate GR, Fritz P, Espinoza JR (2005) Estudio hidrogeológico de los acuíferos el Hundido y Cuatrociénegas, Coahuila: Secretaría de Medio Ambiente y Recursos Naturales, Instituto Mexicano de Tecnología del Agua, Comisión Nacional del Agua, Instituto Nacional de Ecología (292 p)

Ross CS (1946) Sauconite, a clay mineral of the montmorillonite group. Am Mineral 31:411–424

Sanchez-Mejorada P (1987) Evaporite deposit of Laguna del Rey. Soc Min Eng Trans 280:1923–1927

Sangameshwar SR, Barnes HL (1983) Supergene processes in zinc-lead-silver sulfide ores in carbonates. Econ Geol 78:1379–1397

Santoro L, Boni M, Mondillo N, Joachimski M, Woodman J (2015) A cold supergene zinc deposit in Alaska: The Reef Ridge case. Geol Soc Am Bull 127:1534–1549

Shaw SF (1922) The ore deposits of Sierra Mojada, Coahuila, Mexico. Am Inst Min Metall Eng Trans 1182-M:1–17

Silver Bull Resources (2017) Silver Bull provides exploration drilling results. Press Release, 22 March 2017 http://www.silverbullresources.com/s/news.asp?ReportID=783428

Stacey JS, Kramers JD (1975) Approximation of terrestrial lead isotope evolution by a two-stage model. Earth Planet Sci Lett 26:207–221

Stephenson SN, Roberts GG, Hoggard MJ, Whittaker AC (2014) A Cenozoic uplift history of Mexico and its surroundings from longitudinal river profiles. Geochem Geophys Geosyst 15:4734–4758. https://doi.org/10.1002/2014GC005425

Takahashi T (1960) Supergene alteration of zinc and lead deposits in limestone. Econ Geol 55:1083–1115

Tritlla J, Levresse G, Corona-Esquivel R, Banks DA, Lamadrid H, Bourdet J, Pinto-Linares PJ (2007) Epigenetic, low-temperature, carbonate-hosted Pb-Zn-Cu-Ba-F-Sr deposits in Mexico: a Mississippi Valley Type classification. Geol Soc Am Spec Pap 422:417–432

Veizer JH, Hoefs J (1976) The nature of $^{18}O/^{16}O$ and $^{13}C/^{12}C$ secular trends in sedimentary carbonate rocks. Geochim Cosmochim Acta 40:1387–1395

Wassenaar LI, Van Wilgenburg SL, Larson K, Hobson KA (2009) A groundwater isoscape (δD, $\delta^{18}O$) for Mexico. J Geochem Explor 102:123–136

Williams PA (1990) Oxide zone geochemistry: Ellis Horwood series in inorganic chemistry. Ellis Horwood Limited (286 p)

Wolaver BD, Crossey LJ, Karlstrom KE, Banner JL, Cardenas MB, Gutiérrez Ojeda C, Sharp JM Jr (2013) Identifying origins of and pathways for spring waters in a semiarid basin using He, Sr, and C isotopes: Cuatrociénegas Basin, Mexico. Geosphere 9:113–125

Zhou J, Chavez HS (2010) Pedogenic carbonates in Texas: stable isotope distribution and their implications for constructing region-wide paleoenvironments. J Sediment 80:137–150